Biophysical Specialization Project, Fall 2007

Detection Of Microcalcifications For Breast Cancer Diagnosis Using SURF Imaging

Mercy Afadzi

December 19, 2007

Professor: Bjørn Angelsen
Supervisor: Svein-Erik Måsøy

Department of Physics

Abstract

This project was intended to demonstrate the use of new ultrasound method which is based on dual-frequency technique called SURF (Second-Order Ultrasound Field Imaging) for enhancing the diagnosis of breast cancer. SURF imaging uses two pulses with different frequencies (a high and a low frequency) where the high frequency rides on top of the low frequency. The high frequency ($10MHz$) is used for imaging and the low frequency ($1MHz$) is for manipulating background scattering and propagation properties of the high frequency.

Early detection of breast cancer is crucial for successful treatment and also for reducing mortality rate. Clustered microcalcifications is an important indicator of early breast cancer since it is a common feature of tumors found in the breast (asymptomatic and symptomatic cancer). This makes detection of microcalcifications crucial for early breast cancer diagnosis.

The method of detecting microcalcifications was demonstrated experimentally by making ultrasound phantoms containing calcium particles of different sizes, that is, $100\mu m$ and $190\mu m$. Agar was used as the bulk substance with $\sim 8g$ of sephadex ($20 - 80\mu m$) or $\sim 6g$ of silicium carbide ($8.3 - 10.3\mu m$) as scatterers. Glycerol ($\sim 15ml$ for adequate speed of sound) and benzioc acid ($25ml$ for preventing bacterial growth) were also added. Conventional ultrasound (vivid 7 scanner with M12L probe) and mammography (Senographe DS acqusition system) were used for imaging these phantom to detect the calcium particles placed in the phantoms. The phantoms were not imaged with SURF due to some problems with the equipment, that is, background noise in the received signal when used for imaging. Phantoms with different concentration of glycerol (10% and 20%) were also made for detection of change in $\beta_n\kappa$ which can be used for characterization of tissues. Images of the phantoms displayed were taking with both conventional ultrasound and mammography. The speed of sound in the phantoms with different concentrations of glycerol were measured with the same ultrasound scanner.

In conclusion, SURF imaging can provide a contrast ratio of nonlinear microcalcifications scattering to nonlinear tissue scattering of $14dB$ when the linearly scattered signal is adequately suppressed by $-34dB$ (thus in theory). In addition, the phantoms produced are good for future experiments. Phantoms with sephadex shows adequate background scattering (on sonograph) comparable to human tissues than the phantoms made with silicium carbide. Particles were detected both by mammography and ultrasound when the size of particles were $190\mu m$. It was

however, a bit difficult to see or not seen at all when the particle size was about $100\mu m$. The speed of sound in the phantom with 10% concentration of glycerol was found to be $1665m/s$ whereby that of the 20% was found to be $1732m/$s.

Phantoms were not tested with the SURF imaging due to the above mentioned problem but in the future, phantoms could be imaged with SURF to see if the calcium particles could be detected with increased contrast and also if there is change in $\beta_n\kappa$ in the two phantoms with different concentrations of glycerol.

Preface

This report is submitted to the Department of Physics at the Faculty of Natural Sciences at NTNU in fulfillment of student specialization project in the fall semester in the year 2007.

The project was carried out at the Department of Circulation and Medical Imaging at the Faculty of Medicine at NTNU. Supervision of this project was done by Professor Bjørn Angelsen and Post. doc. Svein-Erik Måsøy. The lab work was done together with a colleague called Johan Pääaho Svanem who also worked with the same supervisors on Diagnosing Cancer with SURF imaging. SURF imaging equipment could not be used for this project as it was intended to be because there were noise in the received signal when used for imaging.

I would like to give thanks to God for successful completion of this project. I would also like to express my deepest gratitude to my two supervisors for being helpful, inspiring and dedicated to this project. They never refused giving their time and advice when needed especially Svein-Erik Måsøy. Sincere thanks goes to Thor Andreas Tangen for his contributions and support especially at the lab. Also to my co-worker Johan Pääaho Svanem for his cooperation at the lab. It is nice working together with you. I am grateful to Professor Tore Lindmo and Professor Catharina Davies at the department of physics NTNU for their advice and directions for this report.

Finally, thanks to everybody in the ultrasound group and my other colleagues in the department for all kinds of contributions.

Contents

List of Figures

Chapter 1

INTRODUCTION

The purpose of this study is to enhance the detection of microcalcifications in breast tumors using a new ultrasound imaging method called SURF (Second-Order Ultrasound Field Imaging), which is based on a dual-band technique for the diagnosis of breast cancer. The project was planed as follows;

- Literature study on morphology and physiology of breast cancer.
- A study on acoustical theory to understand the basis of SURF Imaging and how SURF Imaging can improve the diagnosis of breast cancer.
- Making of ultrasound phantoms for the detection of microcalcifications.

Early detection of breast cancer is important in reducing the morbidity and mortality, especially in cases where there are no symptoms (asymptomatic cancer). Also, detection of early stage breast cancer, example higher grade ductal carcinoma in situ (DCIS) (more on DCIS can be found in Chapter 2) is very important because the cancer at that stage is small and have not yet invaded the surrounding stromal tissues. Breast cancer at its early stage is easy to treat whereas it is not easy to treat in its advanced stage. Early diagnosis of breast cancer is mainly done by detection of microcalcifications since it is an important indicator of breast cancer. This makes the detection of microcalcifications important especially for the diagnosis of nonpalpable lesions. For example, DCIS which is an early stage breast cancer can be treated very conservatively with excellent outcome if detected early enough [1, 2].

Currently, mammography is the only standard tool used in breast cancer screening and is able to detect up to 90% of the cancers even before the cancer show some

symptoms [1, 2, 3, 4]. The main feature used by mammography to detect breast cancer is calcifications within the breast tissue or tumor. Although mammography is highly sensitive, it is not very specific in the evaluation of breast microcalcifications, that is, benign calcifications cannot always be distinguished from those indicating malignancy. It is only in 20-35% of the cases that the tumor can be said to be cancerous after needle biopsy [5]. Calcifications are therefore grouped based on assessment of their shape, size, number, morphology and distribution as recommended by the American College of Radiologist, in the Breast Imaging Report Data System (BI-RAD) [1].

Conventional Ultrasound (US) is primarily used to help diagnose breast abnormalities detected by a physician during breast examination and also to characterize potential abnormalities seen on mammography. Thus US can determine if an abnormality is solid (non cancerous or cancerous) or fluid-filled, example cyst. US is also used to guide biopsy procedures because it provides real-time images. However, it is less sensitive for the detection of microcalcifications than mammography. Malignant calcifications with clusters larger than $10mm$ are much more visible on sonographs than benign calcifications [5]. This implies that US can be used to visualize large clusters of microcalcifications that have high probability of being malignant [6, 7]. This is a result of the fact that most malignant calcifications occur within masses which has a hypoechoic background which enables identification of hyperechogenic punctuated calcifications [6, 7, 8]. Thus calcifications located inside echogenic fibroglandular breast tissues are not visible on US images because of the difficulty in differentiating them from echogenic interfaces among tissues, example calcifications found in DCIS [5, 6, 7].

Nevertheless, this cannot be used to distinguish between benign and malignant disease because US can detect calcifications in some benign lesion while it cannot detect some malignant lesions. The smaller the calcifications, the lower the the probability of US detecting them. It is now known that the use of high-frequency transducers can yield a higher percentage of mammographically visible calcifications than could the previously used lower-frequency transducers. The low capability to visualize microcalcifications remains a major limitation for using US as a screening or diagnostic tool for breast cancer. [5, 7, 4].

SURF imaging aims to overcome this limitation, because with SURF imaging one can get better contrast between the tissue and the microcalifications. Thus by adequately suppressing the linearly scattered signal from the tissues by $-34dB$, we can get a contrast ratio of nonlinear microcalcifications scattering to nonlinear tissue scattering [9] to be $\sim 14dB$. As a result malignant microcalcifications may be differentiated accurately from benign ones since there is an increase contrast between the tissue and the microcalifications. This can reduce the number of

needle biopsies, surgery and mammography since these diagnostic tools have some negative effects (exposure to ionising radiation, pain , psychological trauma etc.) on the patient. Also , early detection of breast cancer will be increased if very small microcalcifications are detected.

This report is organized as follows: Chapter two and three explains the theoretical background of the study. That is, anatomy of the female breast and breast tissue composition, types of breast cancer and the different types of breast calcifications can be found in chapter two. Acoustical theory of ultrasound, the basis of SURF Imaging, ultrasound in breast cancer diagnosis and then theoretical bases of ultrasound phantoms is explained in the third chapter. Chapter 4 describes the materials and method used in making the phantoms and then characterization of the phantoms. The fifth chapter gives the results obtained from all the experiments whereas chapter 6 is about how these results were interpreted, that is, discussions on the results. Conclusion of the project has been given in chapter seven.

Part I

BACKGROUND THEORY

Chapter 2

BREAST CANCER

Breast cancer is a cancer of the glandular breast tissues. In other words, malignant cell growth in the glandular breast tissue and is normally seen in women above age 40 and about 1% is also found in men (DCIS) [10, 11]. It is the most common type of cancer in women (3 times more common than all gynecologic malignancies put together), the leading cause of cancer death in women, 1% of all cancer death in men and the fifth most common cause of cancer death worldwide. In 2005 for example, breast cancer caused 502,000 deaths which is about 7% of all cancer deaths and about 1% of all death worldwide [12, 11, 13]. Although nobody knows the exact cause of breast cancer, according to MedicineNet, research have shown that the main risk factors are: personal history of breast cancer, certain breast changes, gene changes, reproductive and menstrual history, race, breast density, being obese after menopause, alcohol, lack of physical activity and finally aging (genetic abnormalities that happen as a result of the aging process and life in general).

In this chapter, the normal female breast tissue is described in the first section whereby the next section describes the various tumors normally found in the breast. That is, it distinguishes benign tumors from malignant tumors. The next section explains the various calcifications that are found in the breast and also explanations of how these calcifications are grouped using BI-RAD standards.The next section gives some charateristics of breast tumors that can be utilized for diagnosis of breast cancer.

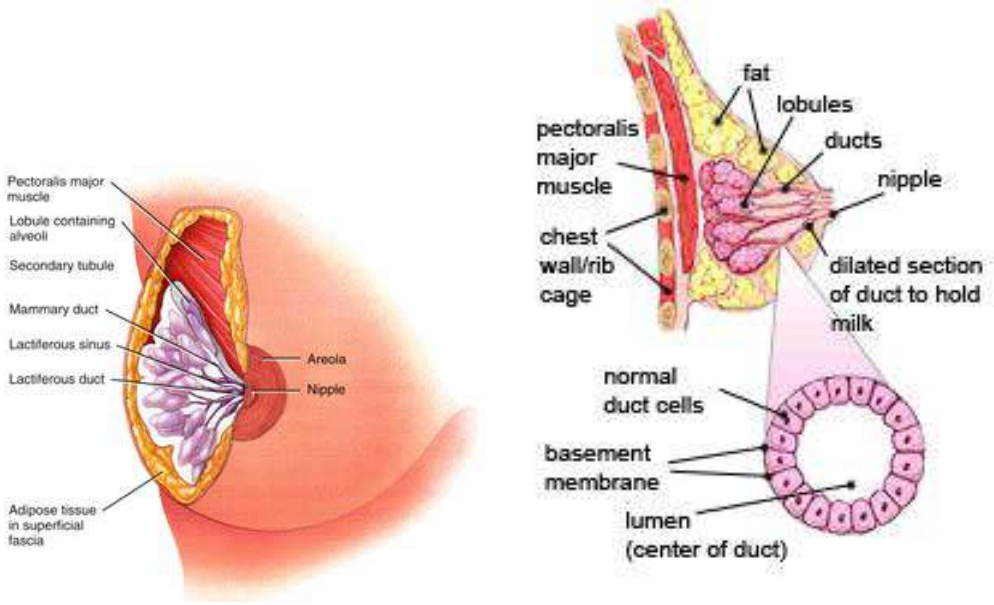

(a) (b)

Figure 2.1: *The normal female breast anatomy (a). Breast profile (b) [13]*

2.1 GROSS ANATOMY OF BREAST

The human breasts are modified sweat glands, producing milk in females. It has an eccentric configuration with the long axis diagonally placed on the pectoralis major muscle and extends into the axilla. Anatomically, the breast is the specialized human tissue which is attached to the front of the chest wall on either side of the breast bone by ligaments [14]. Thus they rest on the major chest muscle (pectoralis). It has no muscle tissue; however, the gland is surrounded by a layer of fat that extends throughout the breast and it's the fat which gives its shape, size and compressibility. See Fig.2.1. The development of the breast is controlled by three major hormones, that is, estrogens, progesterone and prolactin [14] which causes glandular tissues in the breast and the uterus to change during the menstrual cycle. The female breast is spherical and the size varies with age, menstrual cycle and lactation. The breast rests on a rich vascular and lymphatic network within the pectoralis fascia. This represents the retromammary space which is positioned between the deep pectoralis fascia and the superficial pectoralis fascia.

The nipple is located at the center of the breast and it is either flat or angled, that is, less than 180 degree. The smooth dark area surrounding the nipple is the areola.

The lymph vessels of the breast leads to small, round organs called lymph nodes

which are found near the breast in the axilla (underarm), above the collarbone, in the chest behind the breastbone, and in many other parts of the body. The lymph nodes trap bacteria, cancer cells or other harmful substances. The lymphatic flow from the breast is along the course of the branches of the external thoracic veins towards the axial and internal mammary regions. The lymphatic is a route for the access to the vascular system and so tumors can move to other parts of the body through the lymphatic vessel. The lymphatic drainage of the breast therefore has diagnostic and therapeutic implications. That is, the presence of a tumor in the lymph node indicates that the tumor has metastatic potential [15]

The pattern of circulation is not symmetric in the left and right breast of an individual. Arterial circulation of the breast is derived from the internal thoracic artery, axially, lateral thoracic artery and posterior intercostals arteries. Venous drainage is more variable than the arterial supply, but it tends to follow the distribution of the arterial circulation. Deep venous drainage is largely through perforating branches of the internal thoracic vein [14].

2.1.1 Localization Terminology

Each breast can be divided into four quadrants which corresponds to the face of a clock. The names of the quadrants are; the upper outer quadrant (UOQ) which extends towards the axilla is also known as axillary tail, the lower outer quadrants (LOQ), the upper inner quadrant (IUQ) and then the lower inner quadrant (LIQ). These four positions represents the four positions on the clock (12, 3, 6, and 9 o'clock). For example, The 4 o'clock position on the right breast (LIQ) represent the 8 o'clock position on the left breast (LIQ) [16].

The breast can also be divided into four regions namely; posterior region which is closest to the chest wall, the middle region which corresponds to the middle of the breast, the anterior region located behind the nipple and then the subareola region which corresponds to regions behind the areola [16].

2.1.2 Breast Tissue Composition

The human breast has two main types of tissues; glandular tissues and stroma tissues. The glandular part of the breast includes the lobules and ducts where by the stroma tissue includes fatty tissue and fibrous connective tissue (ligaments that support the breast) [17]. The ratio of glands to fat tissue rises from 1:1 in non lactating women to 2:1 in lactating women [17]. There is a wide variation in

the distribution of breast tissues between women but not between breasts within women. The structure of the breast changes throughout life responding to the changes at menarche and menopause and the demands of pregnancy and lactation. In general the amount of fatty and glandular tissue varies with age, that is, glandular tissues predominates in young premenopausal women whereas fatty tissues dominates in older women. In other words, with aging and the changed hormonal milieu that comes with menopause the proportion of fat increases markedly with reduction in the specialized glandular tissue. The breast tissue of a young non lactating woman is however composed of fibro-glandular tissues with little or no subcutaneous fat but as the individual grows the fat is deposited in both the subcutaneous and the retromammary layers [18]. See Fig.2.2

Figure 2.2: *Parenchyma pattern of the human breast* [18].

Lobules:

Each lobe (about 15-20) in each breast is subdivided into numerous lobules. The branching duct system of each lobe ends in clusters of blind-ending terminal ductules lobular unit (TDLU). The TDLU are further divided into the extralobular terminal duct (ETD) and intralobular terminal duct (ITD) which holds the alveolar glands where the milk producing elements (acinus) are found [16]. See Fig.2.3. Lobules are lined by a continuous layer of mammary epithelial and myoepithelial cells. These are columnar or cuboidal epithelial cells, specialized for secretion. Thus the lobular units contain lactocytes (mammary secretory epithelial cells) that synthesize breast milk. It also contains myoepithelial cells which lie in a discontinuous layer underneath the secretory epithelial cells [16]. They respond to oxytocin released by the posterior pituitary. Contraction of myoepithelial cells leads to milk ejection reflex.

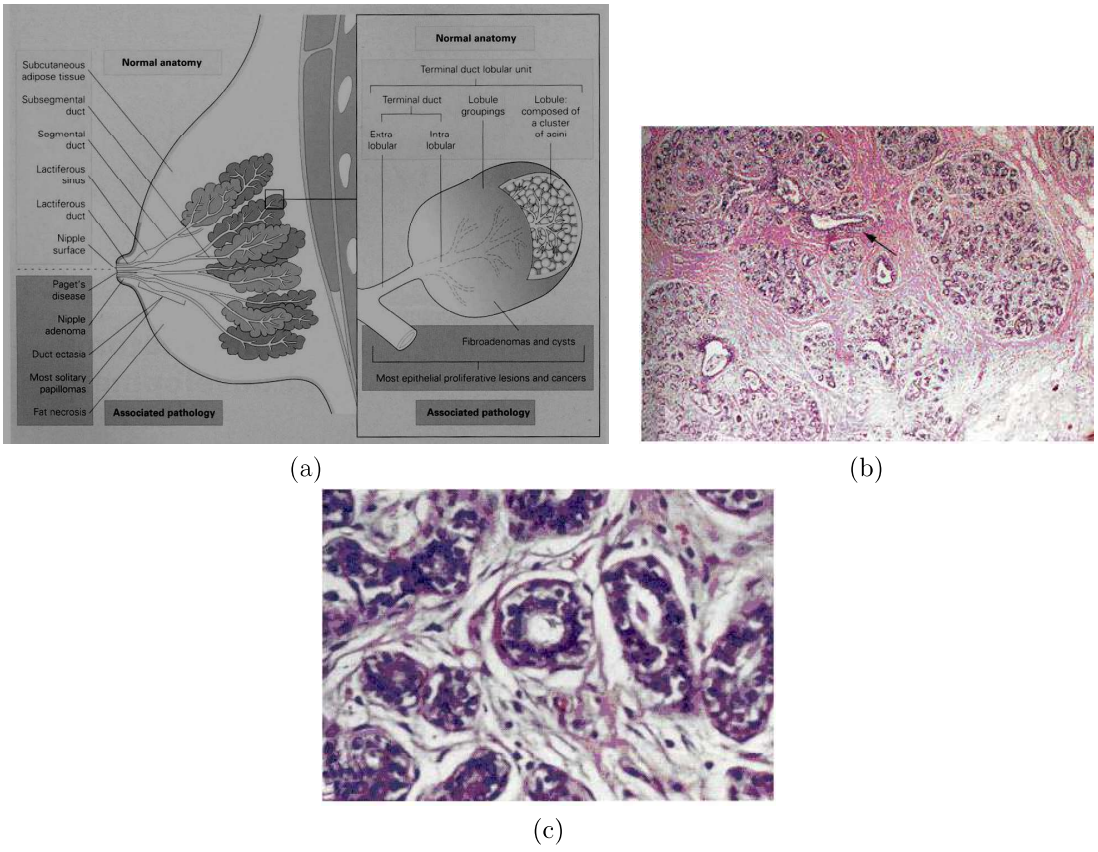

(a) (b)

(c)

Figure 2.3: *Microscopic anatomy of human breast(a). Histology of normal breast tissue of a premenopausal woman ((b) low power photomicrograph of several lobules and few extra-lobular ducts (arrow) and (c) high power photomicrograph of several acini of a lobule [19]*

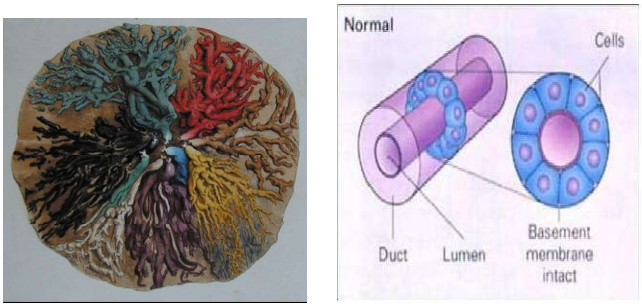

(a) (b)

Figure 2.4: *(a) Artist's impression of the lobes of the breast. The ducts were injected with coloured wax prior to dissection (from Cooper, 1840). (b) A normal duct [17, 19]*

Ductal System

The duct systems of the lobes and lobules are separated from each other by a connective tissue (stroma) containing adipose cells and fibro-collagenous septa. Each lobule can have 10-100 terminal ductules [16]. The milk is collected by distal lactiferous ducts or acini which merge into minor and then major lactiferous ducts. The lactiferous ducts extend into the breast through a series of branches that ends in caliber from the nipple to the terminal ductal-lobular units. The duct system is sealed and surrounded by a basement membrane as illustrated in Fig.2.4.

Stroma:

This is an interlobular tissue also referred to as connective tissue (collagen and elastin), and it contains capillaries and other specialized cells.

Cooper's Ligaments:

These are dense strands of fascia found throughout the entire breast which end on the skin. They are connective tissue in the breast that helps maintain structural integrity but may lose strength and tension at old age.

Basement membrane:

This is an amorphous dense and proteinaceous structure that is present basolateral to the cells in the tissue. It is also called basal lamina and is aligned by fibroblasts. The basement membrane is always in contact with the cells and it provides structural support, divides cells into compartments and regulates cell behavior. Its main constituents are large insoluble molecules that come together to form sheet-like structures.

2.2 TYPES OF BREAST CANCER

Generally, in human tissues, when cells grow old they die and new cells take their place, but if new cells form when the body does not need them, and old cells does not die when they should, then the extra cells form a mass of tissue called tumor which can spread to other parts of the body. Thus in normal cells, cell division balances with cell differentiation and cell death so there is no net accumulation of dividing cells. In tumors, however, cell division does not balance with cell differentiation and cell death which leads to accumulation of cells so that the normal organization and function of the tissues is disrupted.

In breast cancer, mammary epithelial cells has a three dimensional structure and is dependent on a polarized morphology, specialised cell-cell contact and specific attachments to the basement membrane. Also, cellular organization is influence by mechanical forces and signals from neighbouring cells. For proper control of cell proliferation, differentiation, survival, migration and milk-protein section, these features has to function well. Alterations in mammary epithelial cell lose their ability to form organized ducts or alveoli. Malignant transformation of the breast is associated with definable changes in the extracellular matrix (interstitial matrix and the basement membrane) composition and organization which leads to progressive increase in tissue stiffness [20].

Based on the differences in the growth patterns of tumors, they can be classified as either benign or malignant. Benign tumors grow in a confined local area and are rarely dangerous and do not grow back when removed. These tumors do not invade the tissues around them, thus do not spread to other parts of the body. Malignant tumors on the other hand are cancerous and so are generally more dangerous than the benign. They can sometimes reappear after it has been removed and can even spread to damage nearby tissues and organs. The cancer cells can spread by breaking from the original tumor, enter the bloodstream or lymphatic system and invade new organs by forming new tumors and damage the organ, example liver, lungs, and brain (metastasis). Summary of these differences be found in Table 2.1

2.2.1 Benign Breast Tumor

- **Fibrosis:** This is a common benign lesion normally found in women between the ages of 30 and 50. Its also refer to fibrocystic changes or fibrocystic breast condition. It is the most common cause of lumpy breast in women and affects more than 60% of women [11].

Table 2.1: *Differences in the microscopic appearance of benign and malignant tumors[21]*

Trait	benign	malignant
Nuclear size	small	large
Nuclear to cytoplasmic (N/C) ratio	low	high
Nuclear shape	regular	pleomorphic
Mitotic index	low	high
Tissue organization	normal	disorganised
differentiation	well- differentiated	anaplastic
Tumor boundary	well-defined	poorly defined

- **Cysts:** Occurs in terminal duct lobular units when the extralobular terminal duct becomes blocked. That is, they are fluid- filled masses that form at the terminal ductal-lobular unit. A cyst is round, movable and tender to touch and can be easily felt. They may be singular or multiple, ranging in size from a few millimeters to multiples of centimeters. As they grow, they stretch the surrounding tissues which may cause pain and the growth depends on hormonal fluctuations [16].

- **Epithelial hyperplasia:** It is know as proliferative breast disease. This is an overgrowth of the cells that line either the duct (ductal hyperplasia) or the lobules (lobular hyperplasia). It is the most common lesion found in the breast in women over 30 years of age [22].

- **Adenosis:** This refers to enlargement of breast lobules which contains more glands than usual. If many enlarged lobules are found near one another, then adenosis may be felt.

- **Fibroadenoma:** These are benign tumors made up of both glandular breast tissues and stromal tissues. They are estrogen stimulated and are found mostly in women under age 25. They are round with borders that are distinct from the surrounding breast tissue and may contain calcifications. They feel like rubber and move easily, and usually painless. The size of the tumor is under 3cm, the number is multiple in 10-20% [16]. See Fig.2.5.

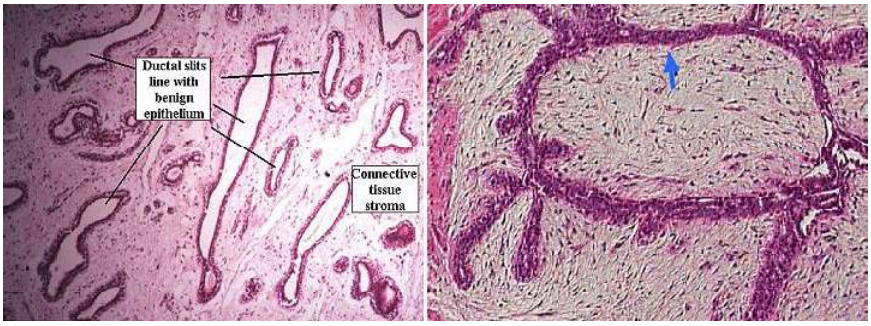

Figure 2.5: *Fibroadenoma;* ***left****, shows slit like and elongated glandular spaces lined by benign epithelium.* ***right****, shows the compressed (blue arrow) duct structures separated by a loose cellular stroma. The black arrow shows the sharply demarcated borders of the lesion* [23].

- **Cystosarcoma phylloides:** They are also called phylloides tumors, forms about 1% of all tumors in the breast. This lesion is the most common nonepithlial (stromal) lesion. See Fig.2.6. The mass is very large and can comprise the entire breast. They are found mostly in women at age $30-40$ and about 10% are malignant so can metastasize to the lungs [24].

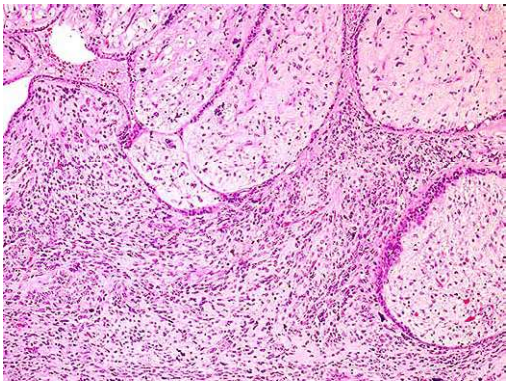

Figure 2.6: *Cystosarcoma phyllodes: Histologic section, Hematoxylin and Eosin stain* [25].

- **Intraductal papilloma:** An intraductal papilloma is a proliferation of epithelial tissue within a duct or cyst that produces a mural nodule. These tumors are typically small and retroareolar. They are often undetectable but sometimes palpable. It is seen in women between the ages of 30 and 55 years.

- **Fat necrosis:** This occurs when an area of the fatty tissue is damaged, thus as a result of surgery or radiation therapy, biopsy or injury. The appearance is firm, slightly fixed mass with skin retraction in 50% of the cases. The mass may show calcifications, which gives the eggshell-like appearance on mammogram [16] see Fig.2.7.

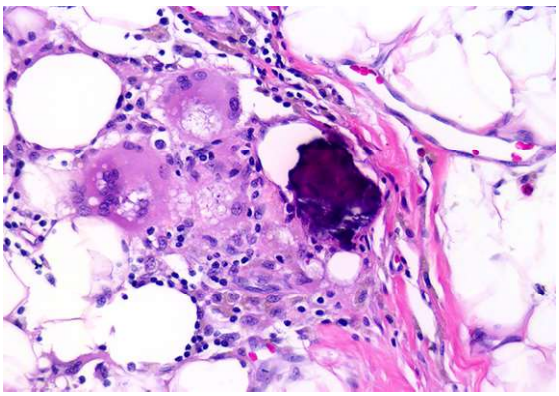

Figure 2.7: *Fat necrosis with microcalcifications. Histologic section (Hematoxylin and Eosin stain) [25].*

2.2.2 Malignant Breast Tumors

The most common types of breast cancer originate from either the epithelial cells of the milk duct (ductal carcinoma) or lobules (lobular carcinoma) and can be non-invasive or invasive. The two main types of breast cancer are ductal or lobular carcinomas. These two types can be invasive or non-invasive depending on the stage of the cancer. Non-invasive also known as 'in situ' cancer are those whereby the cancer cells confine themselves to the ducts or the lobules and do not spread to the surrounding tissues in the breast or other parts of the body. That is, they are confined within the boundaries of the basement membrane but can develop into more serious invasive cancer as can been seen in Fig.2.8. The non-invasive account for 15% of all breast cancers. In invasive cancers, the cells break through normal tissues barriers and invade surrounding tissues that support the ducts and the lobules of the breast. This type of cancer can travel to other parts of the body such as the lymph nodes [26]. Ductal carcinoma account for 90% of all breast cancers, thus the most common, whereby lobular carcinoma account for only 5-10%. Breast cancer is often seen on the mammogram as a stellated lesion or as microcalcifications [16].

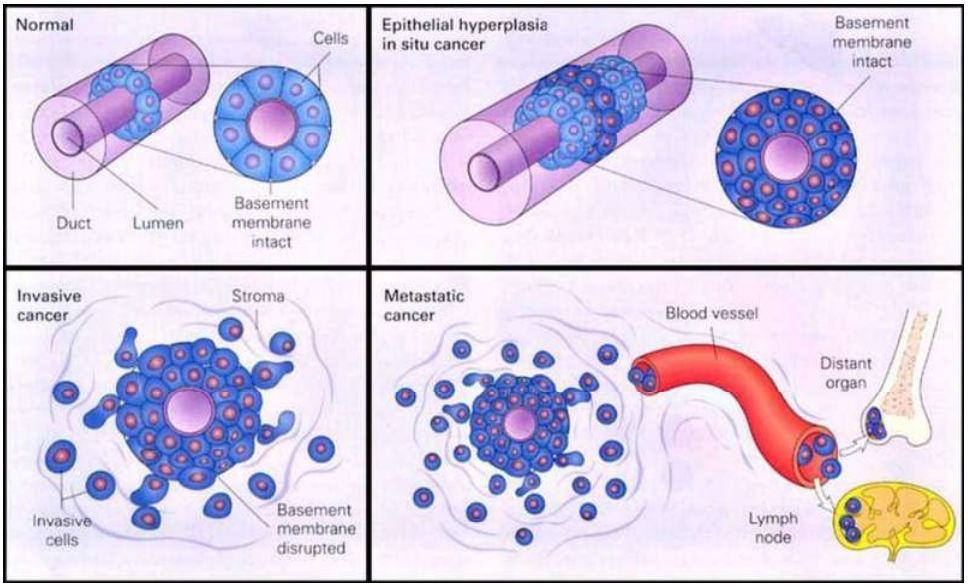

Figure 2.8: *Breast cancers cells begins as single (or more) which have lost normal regulation of differentiation and proliferation but are confined within the basement membrane of the duct or lobule. As these cells go through several proliferations or division, at some point they invade through the basement membrane of the duct or lobule and ultimately metastasize to distant organs* [19].

2.2.2.1 *Non-invasive carcinoma*

Ductal Carcinoma In-Situ (DCIS)

It is an early- stage (stage 0) and so it can also be referred to as 'precancerous' condition or Tis, that is, 'in situ'. It refers to malignant epithelial cells proliferation which accumulate within the lumen of the duct without invasion through the basement membrane. Thus, abnormal cells are still intact in the in the lining of a milk duct and have not yet invaded the surrounding breast tissue, they can grow to cover small or large area of the breast. DCIS can be of any size and can be located in any area inside the breast. The main area of DCIS might add up to $5.0 \times 4.5 \times 3$ mm [27]. DCIS is a heterogeneous lesion which can contain different subtypes. They can be graded as low, moderate and high based on the nuclear size and how the cells differ from normal cells. Although it can consist of several subtypes, usually one of the subtypes predominates. It has been shown that nearly all invasive breast cancers arise from in situ carcinomas. This type of cancer account for 22-23% of all non palpable tumors detected on the mammogram and majority of them show microcalicifications, that is, casting type [28, 16] (more

about casting type can be seen at the next Section).

Examples of low and moderate grade DCIS are;

- **Solid DCIS:** Cancer cells completely fill the affected breast ducts *i.e.* they grow wall-to- wall.
- **Cribiform DCIS:** There are gaps between cancer cells in the affected breast ducts.
- **Papillary DCIS:** The cancer cells are arranged in a fern-like pattern within the ducts. See Fig.2.9

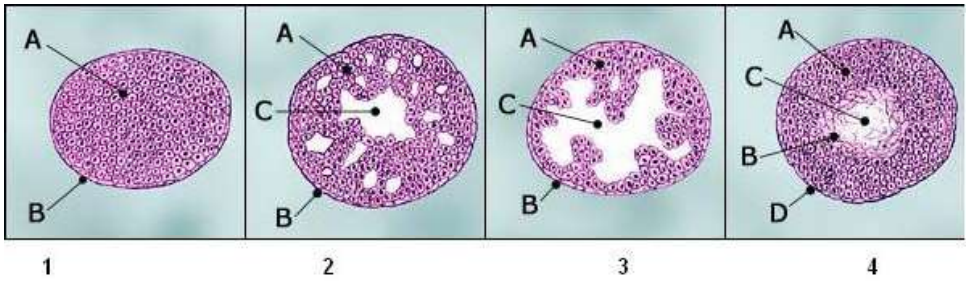

Figure 2.9: *1.Solid, 2.Cribiform, 3.Papillary (A. Cancer cells, B. Basement membrane , C. Lumen) 4. Comedo: A. Living cancer cells, B. Dying cancer cells, C. necrosis, D. Basement membran*e [26].

The low grade DCIS are slow-growing cells, they do look like the normal cells, that is, well differentiated. They have an area of $44.14\mu^2m$ and a perimeter of $25.94\mu m$ [27]. The grade two cells grow faster than normal cells and do not look like them. They have an area of $47.77\mu^2m$ and a perimeter of $27.12\mu m$. Grade three cells however, are fast growing, has necrosis and do not look like the normal cells, that is, poorly differentiated with large nuclear size. The area is $72.05\mu m^2$ and a perimeter of $33.66\mu m$, an e.g. is comedo [27]. See Fig.2.10

Lobular Carcinoma In Situ (LCIS)

In this type of cancer, abnormal cells fill the lobules of the breast but have not yet invaded the surrounding breast tissue. In other words, it arises in the epithelium of the blunt ducts of the mammary lobules. Normal lobular architecture is maintained but the lobules increase in size due to the abnormal cells contained in the lobules. It account for about 1/4 of the non invasive cancers, with an increased occurrence during the reproductive years. It is five time more likely to occur in patients with

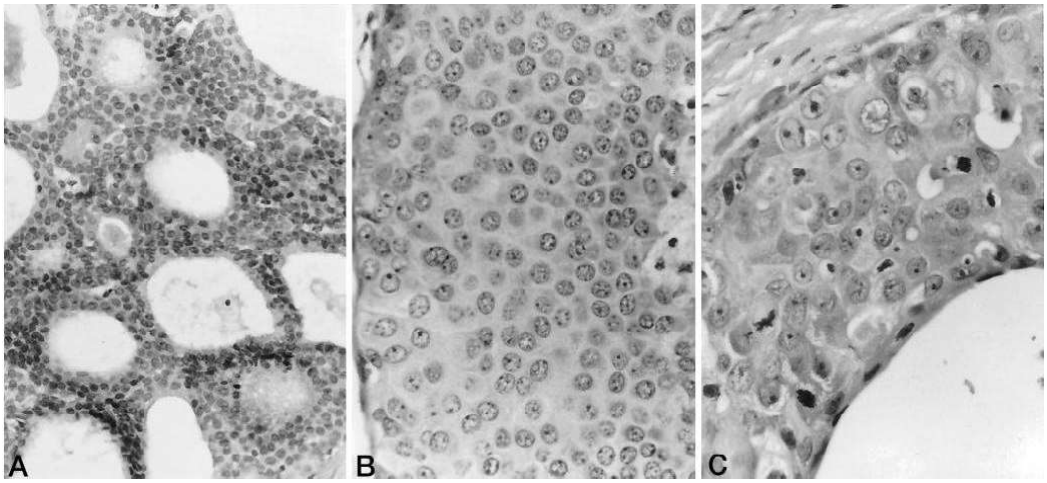

Figure 2.10: *A. low nuclear grade ductal carcinoma in situ (DCIS) shows relatively uniform cells with spherical vesicular nuclei and indistinct nucleoli. B. intermediate nuclear grade DCIS shows moderate nuclear variation with visible nucleoli. C. high nuclear grade DCIS displays pleomorphic cells with enlarged nuclei, prominent nucleoli, and mitoses. (hematoxylin and eosin staining; magnification: A = 100x, B and C = 200*x) [27].

DCIS and in 50% of the cases it can not be seen on the mammogram [16] but are incidental finding at biopsy. This type of cancer has a higher risk of becoming invasive cancer as show in Fig.2.12.

2.2.2.2 *Invasive carcinoma*

Invasive ductal carcinoma (IDC)

This type of cancer represent the largest group of malignant breast tumors, that is, about 65% to 80% of all breast cancers is IDC [29] and account for 65-71% of all cancers [16]. With this, the cancer cells from the lining of the milk duct break free from the duct wall and invade surrounding stromal tissues and may or may not extend into the pectoral fascia and muscle. Thus if a DCIS is not treated the cancer cell can overgrow and then finally move to other organs of the body as illustrated in Fig.2.11. The cancer cells may remain localized (staying near the site of origin) or they can spread even further throughout the body through the blood stream or lymphatic system. The peak age for this cancer is 50 years and are usually palpable.

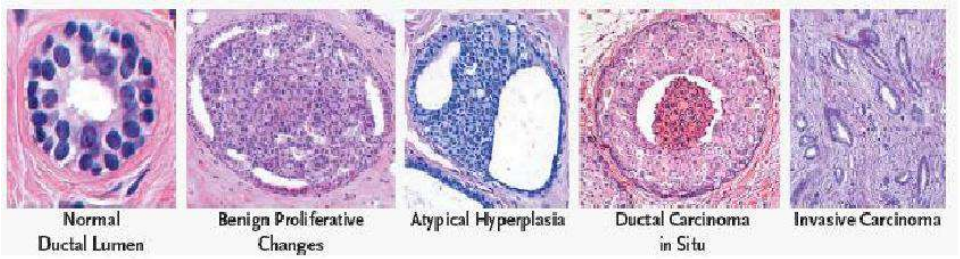

Figure 2.11: *The range of growth from normal to invasive cells*[28].

Invasive Lobular Carcinoma (ILC)

Invasive lobular carcinoma, also starts from the milk producing lobules and invades the surrounding breast tissue and can even spread to more distant parts of the body. It accounts for about 10% of all cancers [16]. This type of breast cancer acts like the IDC. . With ILC, there might not be a lump, but a sensation that the tissues feel different, focal breast thickening but is not associated with microcalcifications [16]. Invasive lobular carcinoma is bilateral in 6% to 28% of cases and is often multicentric but is difficult to perceive on radiographs [16]. See Fig.2.12

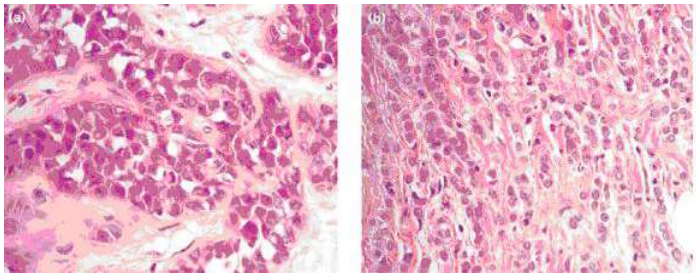

Figure 2.12: ***left.*** *Lobular carcinoma in situ.****right.*** *Invasive lobular carcinoma [30]*

2.3 BREAST CALCIFICATIONS

Breast calcifications are tiny calcium deposits found within the breast tissue. Although they are common, they can not be felt but rather are seen as white spots detected on a mammogram. Calcifications in the breast are very common and in most cases are harmless, that is, they may or may not be associated with a tumor [16] and so they need to be evaluated separately from any associated tumor. However the detection and characterization of calcifications are very important for the diagnosis of non palpable lesions. Thus nonpalpable breast lesions are often detected as calcifications alone, calcifications with architectural distortion or calcifications associated with a mass. For symptomatic cancer, which may be present as a mass lesion, the detection of calcification cannot be the only criteria for the diagnosis since the malignancy can be confirmed by other diagnostic modalities like needle biopsy or surgical excision [1, 2].

Calcifications are therefore grouped based on assessment of their shape, size, number, morphology and distribution as recommended by the American College of Radiologist, in the Breast Imaging Report Data System (BI-RAD) [1]. They can be clustered as seen in multiple calcifications, single, unilateral or bilateral. A cluster is made up of 3-5 calcifications within an area not lager than $0.5 - 1cm^2$ [16]. These calcifications are grouped into three types namely; benign, intermediate concern calcifications and higher probability of malignancy. Benign calcifications are generally round, smooth, dense, scattered over a large area, bilateral or associated with some benign processes whereby malignant calcifications appear as either linear or clustered. The clustered ones are normally at least $4 - 5$ in $1cm^3$ area and are pleomorphic or punctuate, that is, tiny dots less than 1mm which resembles salt. Calcifications associated with breast cancer are usually $\leq 0.5mm$ [15]. Linear calcifications are those that form cast of the duct where by those calcifications that are neither benign nor malignant are considered indeterminate calcifications [1]. In general the smaller the calcification, the greater the suspicion [15].

Generally,breast calcifications can be grouped as macro and micro calcifications.

- **Macro calcifications:** These are coarse calcium in the breast and are usually non cancerous and they form as a result of old injuries, inflammations or aging. This type of calcification is very common in about half of the women over age 50 and 10% of women under age 50 [31]. They are seen on mammograms as large white dots or dashes. They are not harmful and therefore do not need and monitoring [31]

- **Micro calcifications:** These are as a result of the residue left by rapidly dividing cells. That is, specks of calcium that may be found in an area of rapidly dividing cells. They appear as tiny dots or fine specks that are either scattered or clustered; they may be associated with either benign or malignant (cancerous) processes [31].

2.3.1 Some Causes of Breast Calcifications

- Cystic changes, that is, a micro cyst can contain milk of calcium . They are usually mobile and normally takes the shape of the cavities where they are located.
- Arteries and veins can also become calcified. They are distinct and seen on mammogram as two parallel lines or broken tubular patterns.
- Breast surgery and radiation therapy; tubular appearance.
- Benign conditions; Fibroadneoma, sclerosing adenosis, ductal epithelial hyperplasia and ductal ectasia

Radiologically, calcifications can be divided into benign, intermediate concern, and higher probability of malignancy according to the morphology and the distribution [1].

2.3.2 Characteristics of Breast Calcifications

2.3.2.1 *Benign*

Generally, benign breast calcifications are large (greater than 1mm), smooth, round, dense, scattered over a large area, or may be bilateral. See Fig.2.13

- Smooth contours, high uniform density, example, plasma cell mastitis.
- Evenly scattered homogeneous or vascular calcification, example, calcified arteries.
- Sharply outline, spherical, or oval, example, oil cysts.
- Pear-like densities - resemble teacups or pearl drops on the lateral projection, example, milk of calcium. This is caused by calcium deposit floating within the lumen, example, fibrocystic changes.

- Ring-like, hollow, example, Sebaceous gland calcifications
- Eggshell-like usually are $\leq 1mm$ on side view, example, oil cyst, paplilloma. See Fig.2.13
- Large, bizarre size, example Hemangiomas.
- Lucent centered deposits of skin calcifications. See Fig.2.13

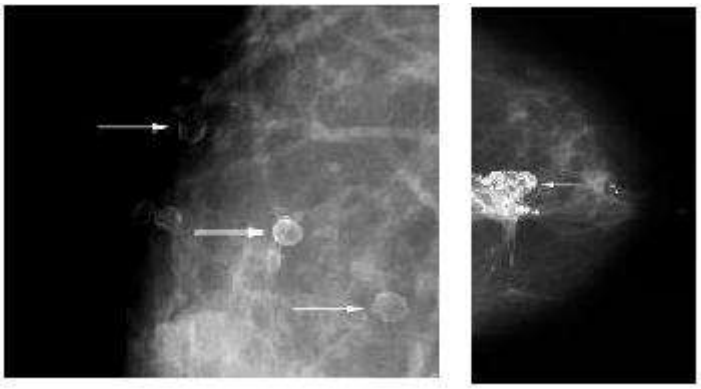

Figure 2.13: *Benign breast calcification: Eggshell or rim calcifications have walls thinner than those of lucent-centered calcification* [32].

2.3.2.2 *Intermediate concern, suspicious calcifications*

- Amorphous or indistinct calcifications which are often round or 'flake' shaped or hazy in appearance.
- Coarse heterogeneous calcification-irregular conspicuous calcifications that are larger than 0.5mm

2.3.2.3 *Malignant calcifications*

Malignant calcifications show clustered (at least $4-5$ calcifications in $1cm^2$ area) or linear (include branching) morphology [1]. Three basic types of malignant calcifications are:

- **Casting-type calcifications;** they appear mammograhically as fine linear branching calcifications that are fragmented with irregular contours. These are produce when carcinoma in situ fills the ducts and their branches. The uneven production and the irregular necrosis of the cellular content give the shape of the cast. The cast has a contour with irregular density, size and length and are always fragmented. The width of the ducts determines the width of the castings. High-grade(Comedo) Ductal carcinoma in situ (DCIS) is frequently associated with casting-type micro calcifications [16]. See Fig.2.14

- **Granular-type calcifications:** these are irregular in form, size, and density. They appear on a mammogram as granulated sugar or crushed stones and are usually grouped closed together in single or multiple clusters. A typical example is low grade (cribiform) DCIS [16].

- **Powderish calcifications:** with this type the individual calcifications can not be seen because they are too small to be seen but the entire cluster is visible on a mammogram. That is, they appear in multiples [16].

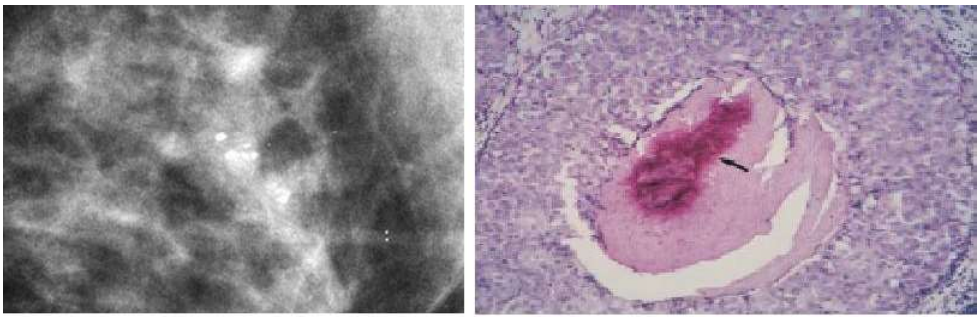

Figure 2.14: ***left,*** *Mammogram of higher grade DCIS with microcalcifications* ***right,*** *high grade DCIS with central necrosis and calcification (arrow) within an enlarged duct (magnification = 100; hematoxylin-eosin [H-E] stain)* [33].

2.4 CHARACTERISTIC OF BREAST TUMORS THAT CAN BE UTILIZED FOR DIAGNOSIS

1. Most breast tumors show clustered microcalcifications. Thus both in the benign and malignant ones but they both have distinct features as described

in the previous section. Even some of the the pre-cancerous and the nonpalpable ones show microcalifications, example, DCIS and LCIS [33] .

2. Most breast tumors are palpable thus they form a solid mass or lump in the affected breast and also have definite size depending on the stage of the cancer.

3. There is an increased tissue stiffening in the malignant tumors than in benign tumors [20].

4. About 90% of all breast tumors starts the epithelial cells of the lobules and the ducts. That is, the number of carcinomas out weighs that of sarcomas.

5. Ductal carcinoma accounts for 90% of all breast cancers.

6. Breast cancer is normally found in women about age 40 where the breast tissues are mainly composed of fat [17]. See Fig.2.2

7. Malignant tumors has greater number of vessels and vessel architecture differs from the morphology of benign lesions.

Chapter 3

ULTRASOUND THEORY

3.1 ACOUSTIC THEORY

The name ultrasound (US) is used to describe sound waves with frequencies above the audible range, that is, above $15-20$kHz. US imaging is based on the same principles involved in the sonar used by bats, ships and fishermen. When a sound wave strikes an object, it bounces backward, or echoes, by measuring these echo waves it is possible to determine how far away the object is, its size, shape, consistency (whether the object is solid, filled with fluid, or both) and uniformity.

Medical US usually operates in the range $2-10$ MHz [34]. Low frequencies are used to image internal structures of the body (*liver*) where by high frequencies are used for supperfacial structures (*breast*). In medicine, ultrasound is used to detect changes in appearance and function of organs, tissues, or abnormal masses, such as tumors. Currently, US imaging is widespread in clinical use and it accounts for about one in four of all imaging procedures worldwide [35].

This chapter deals with the acoustical theory of US and SURF Imaging. Thus the mathematical description of interaction of waves with tissues which produces linear and nonlinear wave equation can be found in the first section. This was followed by the theory of SURF Imaging, especially how it can be use to produce contrast between the tissues and calcium particles. The next section describes some of the limitations of the conventional US in breast cancer diagnosis and finally theory of US phantoms.

3.1.1 Interaction of Ultrasound with Tissues

Interaction of Ultrasound waves with organs and tissues can be described in terms of reflection, scattering, refraction, and attenuation. The basis of US is reflection of the transmitted ultrasound signal from internal structures. Thus images are produce due to reflections of the back scattered waves from the tissues interfaces due to the difference between the characteristic impedances of the two materials which also depends on the propagation velocity and the mass density of the tissue [34].

3.1.1.1 *Homogeneous linear wave equation*

In a homogeneous and isotropic material, that is, a material where by acoustic parameters (mass density and compressibility) are independent of position and direction in the material, the propagation of sound waves is due to the elastic properties of the medium. Example in biological tissues the propagation of sound waves produces compression or shear waves. The compression type are longitudinal waves, in other words, the particle's displacement is along the direction of the wave propagation. These longitudinal waves are caused by a cyclic compression and expansion of the tissue which is accompanied by pressure increase or decrease.

Assuming a linear relationship between compression and pressure yields:

$$\frac{\delta v}{\Delta V_O} = -\frac{\partial \psi}{\partial z} = \kappa p + (h \otimes \kappa p) \tag{3.1}$$

$\frac{\delta v}{\Delta V_O}$ is the volume compression. ψ is the particle displacement the convolution term $((h \otimes \kappa p))$ is the absorption term. κ is the compressibility and ρ is the mass density of the tissue [34].

Also the particle displacement is related to the particle velocity by:

$$\frac{\partial \psi}{\partial t} = u$$

where u is the particle velocity.

Assuming no absorption, the constitutive equation then becomes:

$$-\frac{\partial \psi}{\partial z} = \kappa p \tag{3.2}$$

From Newtons second law, the kinetic energy can be given as:

$$\rho \frac{\partial u}{\partial t} = -\nabla p \tag{3.3}$$

combining Eq.3.2 and 3.3, the propagation of waves in a homogeneous medium (constant mass density and compressibility) can be described by the linear wave equation [34] :

$$\begin{aligned} \frac{\partial^2 p}{\partial z^2} - \kappa \rho \frac{\partial^2 p}{\partial t^2} = 0 \\ \frac{\partial^2 u}{\partial z^2} - \kappa \rho \frac{\partial^2 u}{\partial t^2} = 0 \end{aligned} \tag{3.4}$$

The impulse potential is related to the pressure by the relation:

$$\rho u = -\nabla \varphi \;\Rightarrow\; p = \frac{\partial \varphi}{\partial t} \tag{3.5}$$

That is, the homogeneous linear wave equation can the be written as [34]:

$$\frac{\partial^2 \varphi}{\partial z^2} - \frac{1}{c^2} \frac{\partial^2 \varphi}{\partial t^2} = 0 \tag{3.6}$$

where

$$c^2 = \frac{1}{\kappa \rho}$$

is the propagation velocity which is independent of pressure.

3.1.1.2 *Homogeneous nonlinear wave equation*

Soft tissues is mainly water with a matrix of solid constituents and so there is a small variation in wave propagation velocity between different types of soft tissues. The linear relationship is therefore not valid any longer with increase in pressure, which means the compressibility function can be expressed as a second order approximation.

The relationship between compression and pressure then becomes:

$$\frac{\delta v}{\Delta V_o} = -\frac{\partial \psi}{\partial z} = \kappa p - \beta_n (\kappa p)^2 + (h \otimes \kappa p) \tag{3.7}$$

where β_n is the compressibility nonlinearity parameter.

Using Taylor's expansion and neglecting the absorption term the homogeneous nonlinear wave equation can be written as:

$$\begin{aligned} \nabla^2\varphi - \left\{\kappa\,\rho\left(1 - 2\,\beta_n\kappa\frac{\partial\varphi}{\partial t}\right)\frac{\partial^2\varphi}{\partial\,t^2}\right\} = 0 \\ \Rightarrow \nabla^2\varphi - \frac{1}{c(p)^2}\frac{\partial^2\varphi}{\partial\,t^2} = 0 \end{aligned} \tag{3.8}$$

where;

$$c(p) = \frac{1}{\sqrt{\kappa\,\rho\left(1 - \beta_n\,\kappa\,\frac{\partial\varphi}{\partial t}\right)}} \approx c_o\left(1 + \kappa\,\rho(1 - \beta_n)\right)$$

which is pressure dependent

3.1.1.3 *Inhomogeneous linear wave equation*

Assuming there are other forces acting on the material other than those caused by the compression of the material from the wave, then the generation of the wave is as a result of external forces (surface or body forces) [34].

Hence:

$$\rho\frac{\partial\,u}{\partial\,t} = -\nabla\,p(r,t) + f(r,t) \tag{3.9}$$

combining Eq. 3.2 and 3.9 yields an inhomogeneous wave equation.

$$\nabla^2 p - \frac{1}{c^2}\frac{\partial^2\,p}{\partial\,t^2} = \nabla f(r,t) \tag{3.10}$$

where f(r,t) is the force term. According to Helmholtz' decomposition theorem, $f = \nabla F + \nabla \times G$ but because $\nabla(\nabla \times G) = 0$ only the scalar potential part will excite compression waves hence:

$$\begin{aligned} \nabla^2 P - \frac{1}{c^2}\frac{\partial^2 p}{\partial t^2} = \nabla^2 F \\ \nabla^2\varphi - \frac{1}{c^2}\frac{\partial^2\,\varphi}{\partial\,t^2} = \frac{1}{c^2}\frac{\partial\,F}{\partial\,t} \end{aligned} \tag{3.11}$$

Thus the equation with zero source term is called Homogeneous wave equation where by the one with a source term is inhomogeneous wave equation [34]

The equation can finally be written as:

$$\nabla^2\varphi - \frac{1}{c^2}\frac{\partial^2\varphi}{\partial t^2} = -S(r,t) \tag{3.12}$$

where S(r,t) is the source term.

3.1.1.4 *Wave propagation and scattering in heterogeneous tissues*

The solid constituents of soft tissue is a mixture of different components, example muscle, fat, connective tissue, etc. These constituents have different mass densities and compressibility. This introduces spatial variations of mass density and compressibility on the scale of wavelength which leads to scattering of ultrasound [34].

Thus;

$$\begin{aligned}\rho(r) &= \rho_a + \rho_f(r)\\ \kappa(r) &= \kappa_a + \kappa_f(r)\end{aligned} \tag{3.13}$$

Where, the subscript $a > \lambda$ and$f < \lambda$,
ρ_a and κ_a are spatial averages of $\rho(r)$ (mass density) and $\kappa(r)$ (compressibility) respectively and
ρ_f and κ_f are the spatial fluctuations of the mass density and the compressibility around the average.

Thus, $\rho(r)$ is the uncompressed mass density at zero pressure amplitude but the change in density due to typical pressure compression are much less than variations between different materials.

From Eq. 3.5, the linear wave equation then becomes

$$\nabla\left(\frac{1}{\rho(r)}\nabla\,\varphi(r,t)\right) - \kappa(r)\,\frac{\partial^2\varphi}{\partial t^2} = 0 \tag{3.14}$$

According to Angelsen [34], the mass density can be expressed as:

$$\frac{1}{\rho} = \frac{1}{\rho_a} - \frac{\rho_f}{\rho\,\rho_a} = \frac{1}{\rho_a} - \frac{1}{\rho_a}\gamma$$

inserting this relation into Eq. 3.14 the equation then becomes;

$$\nabla\varphi(r,t) - \frac{1}{c^2}\frac{\partial^2\varphi}{\partial t^2} = \frac{\beta(r)}{c^2}\frac{\partial^2\varphi}{\partial t^2} + \nabla(\gamma\,\nabla\varphi) = -S(r,t) \tag{3.15}$$

which implies that

$$-S(r,t) = \frac{\beta(r)}{c^2}\frac{\partial^2\varphi}{\partial t^2}$$

which is the source term that is responsible for scattering of the ultrasound beam where;

$$\gamma(r) = \frac{\rho_f(r)}{\rho}$$
$$\beta(r) = \frac{\kappa_f(r)}{\kappa_a}$$

3.1.1.5 *Nonlinear wave equation*

The homogeneous nonlinear wave equation, that is,

$$\nabla^2\varphi - \frac{1}{c(p)^2}\frac{\partial^2\varphi}{\partial t^2} - h_p \otimes \frac{1}{c_o^2}\frac{\partial^2\varphi}{\partial t^2} = 0 \tag{3.16}$$

Considering nonlinear propagation in a heterogeneous tissue where there is spatial variations in the mass density and the compressibility of tissue [34]. These variations in the nonlinearity will cause harmonic scattering as shown in the equations below.

Thus,

$$\begin{aligned} \rho(r) &= \rho_a + \rho_f(r) \\ \kappa(r) &= \kappa_a + \kappa_f(r) \\ \beta_n(r) &= \beta_{na} + \beta_{nf}(r) \\ \varphi &= \varphi(r,t) \\ p &= p(r,t) \end{aligned} \tag{3.17}$$

Combining these equations will give the general wave equation as follows [34]:

$$\begin{aligned} \nabla^2\varphi - \frac{1}{c(p)^2}\frac{\partial^2\varphi}{\partial t^2} - h_p \otimes \frac{1}{c_o^2}\frac{\partial^2\varphi}{\partial t^2} = \\ \frac{\beta(r)}{c^2}\frac{\partial^2\varphi}{\partial t^2} + \nabla\left(\gamma(r)\,\nabla\varphi\right) - 2\sigma_n(r)\beta_{na}(r)\kappa_a(r)\frac{1}{c_o}\frac{\partial\varphi}{\partial t}\frac{\partial^2\varphi}{\partial t^2} \end{aligned} \tag{3.18}$$

The first two terms on the left represents nonlinear propagation whereby the convolution term represents absorption. Also on the right hand side, the first two terms represent linear scattering source terms whereas the third represents nonlinear scattering source terms. Here scattering sources including the absorption term have have be neglected since its of low magnitude.

Now separating the propagation and the scattering terms gives [34],
Propagation velocities;

Linear:

$$c_o = \frac{1}{\sqrt{\rho_a \kappa_a}}$$

Nonlinear:

$$c(p) = c_o(1 + \beta_{na}(r)\kappa(r)p(r,t))$$

Scattering parameters;

Linear:

$$\beta(r) = \frac{\kappa_f(r)}{\kappa_a(r)}$$
$$\gamma(r) = \frac{\rho_f(r)}{\rho(r)}$$

Nonlinear:

$$\sigma_n(r) = (2 + \beta(r))\,\beta(r) + \frac{\beta_{nf}(r)}{\beta_{na}(r)}\,(1 + \beta(r))^2\,.$$

As it can be seen, the nonlinear propagation velocity is pressure dependent, which implies that, high pressure oscillations propagates with higher velocities than low pressure oscillations. This produces a nonlinear propagation distortion of the wave oscillation that accumulates with propagation distance and introduces harmonic frequency components in the propagating pulse [34].

The nonlinear elasticity in soft tissue can be described by the second order approximation in Eq. 3.7. which means that the nonlinear propagation velocity and the nonlinear scattering coefficient are:

$$\begin{aligned} c(r) &= \frac{1}{\sqrt{\rho_a\,\kappa_a(1 - 2\beta_n\kappa_a p)}} \approx c_o(1 + \beta_n\kappa_a p) \\ \sigma_n(r) &= \left\{2\beta_{na}(2 + \beta(r))\beta(r) + \beta_{nf}(1 + \beta(r))^2\right\}\kappa_a p \end{aligned} \tag{3.19}$$

where

$$c_o(r) = \frac{1}{\sqrt{\rho_a \kappa_a}}$$

Typical values of acoustic parameters for soft tissues can be found in Table 3.1. This can be use to estimate the value of σ_n [34].

Table 3.1: *Acoustic parameters for soft tissues.* $\kappa(a)$, ρ, c *and* β_{nf} *represent average compressibility, mass density, speed of sound and compressibility nonlinearity parameter respectively.* [34].

Materials	β_n	$\kappa_a[10^{-12}Pa^{-1}]$	$\rho[kg/m^3]$	$c[m/s]$
Fresh water	3.50	452	988	1497
Sea water	3.60	416	1025	1531
Fat	6.00	508	950	1440
Liver	4.34	385	1060	1560
Muscle, Skeletal	4.70	380	1070	1560
Gland	4.5	385	1060	

Maximum values for $\beta(r) \sim pm0.3$ and that of $\beta_{nf} \sim \pm 1.5$. This implies:

$$\sigma_n =\sim 4\beta_{na}\beta(r)\kappa_a p$$

From Eq.3.17 we can see that the nonlinear scattering term is proportional to the linear term $\beta(r)$ so for $\beta(r) \approx \pm 0.1$ and $\beta_{nf} \approx \pm 0.5$. we get $\sigma_n \approx 2\kappa_a p$ [9].

3.1.2 SURF Method

SURF- Second Order Ultrasound Field Imaging is based on dual-band technique. That is, transmitting two ultrasound pulses with a large separation in frequency simultaneously. These two transmitted pulses consist of a low frequency (LF) manipulation pulse and a high frequency (HF) that overlap in the time domain. Thus, the propagating pulse complex can be seen as a high frequency wave surfing on top of a low frequency wave [36]. This is done by combining a low frequency pulse (example 1MHz) with a high frequency (example 10MHz) whereby the low frequency is used for manipulation of tissue properties (scattering) and the high frequency is for imaging . In other words, the scattering properties of the high frequency can be manipulated by the low frequency by varying phase and amplitude of the low frequency for each transmission. An illustration of this phenomena is described in the figure below (10 MHz pulse rides on a low frequency pulse(1 MHz)). The low frequency pulses are inverted between transmissions unlike the high frequency pulse which is equal for both cases [37, 38, 36]. See Fig.3.1

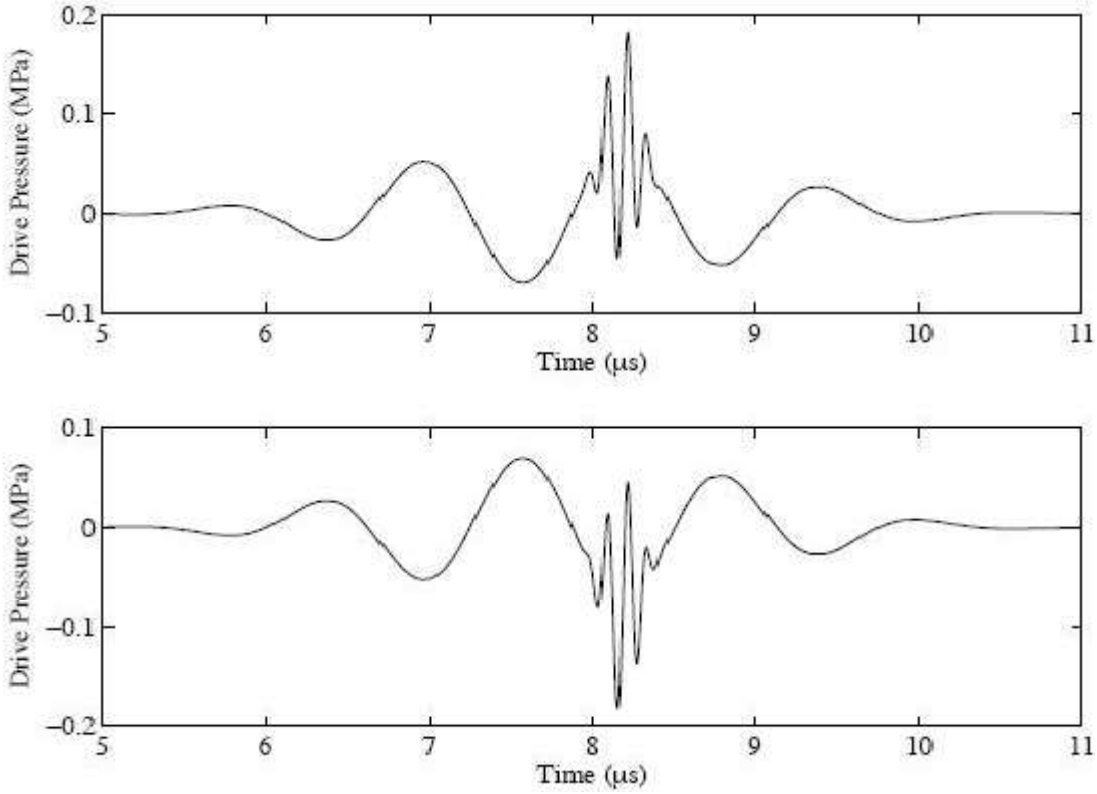

Figure 3.1: *Example of transmitted pulses; Upper panel: High frequency imaging pulse placed in positive low frequency manipulation pressure. Lower panel: High frequency imaging pulse placed in negative low frequency manipulation pulse* [38].

3.1.2.1 *Detection of Nonlinear scattering in soft tissue*

Since the manipulation pulse, that is , the LF is mainly used for altering the scattering properties, it is only transmitted but not received. Thus the difference between these two LF pulses is filtered out by the use of a pass- band around HF on the received signal as shown in Fig.3.2.

In SURF, the total acoustic pressure is given as $p = p_m + p_i$ where m and i are manipulation(LF) and imaging(HF) components of the pressure respectively. This implies that, the nonlinear propagation velocity then becomes:

c(p)= $c_o[1 + \beta_{na}\,\kappa_a\,p_m + \beta_{na}\,\kappa_a\,p_i]$

where; $c_o(1 + \beta_{na}\,\kappa_a\,p_m)$ is from the modulation beam and $c_o(1 + \beta_{na}\kappa_a p_i)$ is from the imaging beam. These are responsible for nonlinear distortion of p_m and p_i

respectively.

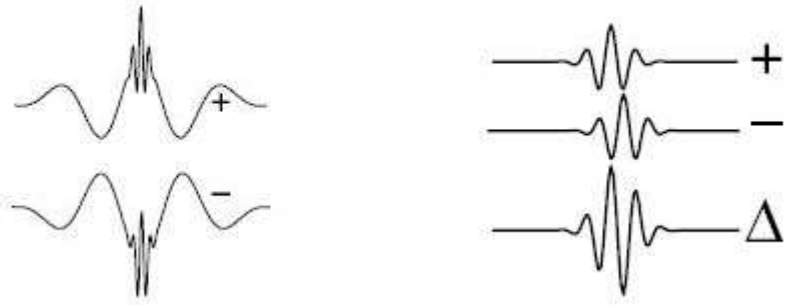

Figure 3.2: ***Left***, *Pulse complexes for positive and negative polarity of the LF manipulation.* ***Rght***, *Two time shifted pulses and their maximum possible difference [36]*

.

According to Måsøy [37], if the frequency ratio HF/LF is high, we may assume the imaging pulse experiences a constant manipulation pressure. That is, the imaging pulse will experiences a speed of sound proportional to the manipulation pressure.

Then $p = p_m$
$\Rightarrow c_i(p_m) = c_o(1 + \beta_{na}\kappa_a p_m)$.

For this reason, the frequency of the HF pulse is normally 10 times that of the LF pulse. Neglecting mixing effects; the nonlinear scattering term in the general wave equation, that is,

$$S_{nl} = -2\sigma_n(r)\,\beta_{na}(r)\kappa_a(r)\,\frac{1}{c_o}\,\frac{\partial\varphi}{\partial t}\frac{\partial^2\varphi}{\partial\, t^2}$$

This shows that $S_{nl} \propto p$.

Also since the imaging pulse is the same for both transmissions, nonlinear high-frequency propagation effects will cancel after subtraction if the pulses are properly aligned and then it would be left with the change in nonlinear scattering due to variation of p_m.

From Fig.3.2, inversion of LF pulse causes the two HF pulses to propagate with different effective speed of sound which generates a relatively small time shift between them at shallow depths but is accumulated during forward propagation. Amplitude reduction of a reflected or scattered LF pulse causes an imaging HF pulse to observe negligible sound speed manipulation after being scattered. This therefore

leads to accumulation of a smaller relative delay than the forward propagating HF pulse [37].

The time delay for the negative polarity is given as, $t_l = \frac{Z}{c_l}$ and that of the positive polarity frequency will be $t_h = \frac{Z}{c_h}$.
the time delay between these two pulses is therefore:

$$\Delta\tau = t_l - t_h = \frac{Z}{c_l} - \frac{Z}{c_h} = Z\alpha \tag{3.20}$$

where; $\alpha = \frac{\Delta\tau}{Z}\frac{c_h - c_l}{c_l c_h}$

Table 3.2: *Typical values of manipulation pressure and the corresponding delay.*

p_m[MPa]	0.1	0.5	1	1.0	2
$\frac{\Delta\tau}{Z}$	2.7	13	27	40	53

The time delay is a function of P, β_n, κ, that is, from $\Delta\tau = f(p, \beta_n, \kappa)$ in Eq. 3.18. This implies that the propagation delay for the backscattered HF pulse from a distance r can also be written as:

$$\begin{aligned} t(r) &= \int_{\Gamma(r)} \frac{ds}{c(s)p_m(s)} = t_o(r) + \tau(r) \\ t_o &= \int_{\Gamma(r)} \frac{ds}{c_o(s)} \\ \tau(r) &= -\int_r \frac{ds}{c_o(s)} \beta_n(s)\kappa(s)p_m(s) \end{aligned} \tag{3.21}$$

Where $\tau(r)$ is the nonlinear propagation delay for the HF pulse produced by the LF pulse, Γ is the path to and from the scatter. This can be used to estimate $\beta_n\kappa$ for characterization of tissues and also to calibrate the pressure p_m as illustrated in the Fig3.3.

From Angelsen [9], the received signal from the LF pulse (both positive and negative polarity) can be modeled as:

$$\begin{aligned} y_+ &= x_l(t - \tau(t)) + x_n(t - \tau(t)) \\ y_- &= x_l(t + \tau(t)) - x_n(t + \tau(t)) \end{aligned} \tag{3.22}$$

Where t is the depth time, x_l is the linear scattered signal, that is, $\beta(r)$ and $\gamma(r)$ and x_n represent the nonlinear scattered signal.

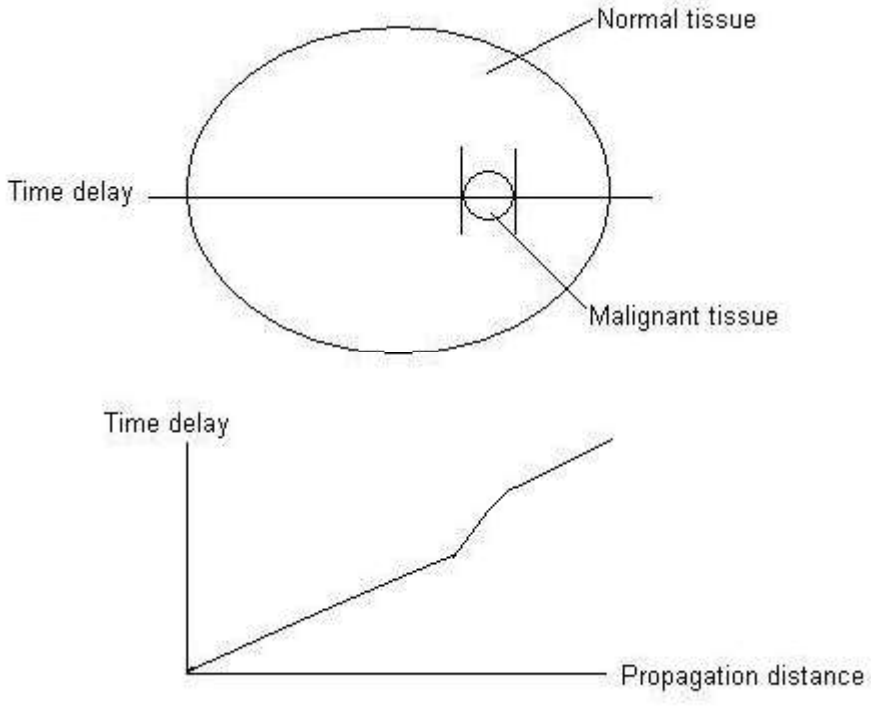

Figure 3.3: *An illustration of the time delay against propagation distance*

Using cross correlation, we can estimate the linear and the nonlinear signals as follows [9]:

$$\begin{aligned} x_{ne} &= \frac{1}{2}\left\{y_+(t+\hat{\tau}(t)) - y_-(t-\hat{\tau}(t))\right\} \\ x_{le} &= \frac{1}{2}\left\{y_+(t+\hat{\tau}(t)) + y_-(t+\hat{\tau}(t))\right\} \end{aligned} \tag{3.23}$$

Linear back-scattered signal received will be: $\sigma \sim 1.3\,\beta(r) \sim \beta(r) - \gamma(r)$

So the ratio of the envelope of the nonlinear to the linear back-scattered signals is therefore;

$$\frac{a_{ne}(r)}{a_{le}(r)} \sim 4\beta_{na}\kappa_a \frac{\beta(r)}{\beta(r)-\gamma(r)}\, p_m \;\sim\; 3\beta_{na}\,\kappa a p_m \tag{3.24}$$

This ratio can be use to estimate quantitative material parameters. For instance for $p_m \sim 1$MPa, the ratio is $\sim -44dB$.

According to Angelsen [9], the nonlinear scattering term for soft tissue (internal) can be approximated to be:

$$\sigma_{n(int)} = 4\beta_{na}\beta(r)\kappa_a p_m \sim 2\kappa_a p_m \tag{3.25}$$

A solid particle in soft tissue, example microcalcifications, one can get $\beta(r) \sim 1$ and $\beta_{na} \sim 5$. This gives a nonlinear scattering coefficient between the soft tissue and the solid particle as:

$$\sigma_{n(part)} = 2\beta_{na}\kappa_a p \approx 10\kappa_a p_m \tag{3.26}$$

Now the ratio between Eq 3.23 and 3.24 gives

$$\frac{\sigma_{n(part)}}{\sigma_{n(int)}} \approx 5 \approx 14dB. \tag{3.27}$$

This implies that a contrast ratio of $\sim 14dB$ can be obtained from the ratio of nonlinear microcalcification scattering to nonlinear tissue scattering if the linear scattering from the tissue is adequately suppressed. If $\kappa_a \approx 400x10^{-12}Pa^{-1}$ and $p_m = 2.5MPa$ we can get deep in the soft tissue and so the ratio of the nonlinear to the linear scattering is :

$$\frac{Nonlscat}{Linscat} = \frac{(2+\beta(r))\beta(r)}{\beta(r)-\gamma(r)} 2\beta_{na}\,\kappa\,p_m \sim 3\beta_{na}\,\kappa_a\,p_m \sim 15x10^{-3} \sim -36dB. \tag{3.28}$$

Which means that by suppressing the linearly scattered signal by at least -34dB nonlinear imaging of the microcalcifications in the tissue can be done.

3.2 ULTRASOUND IN THE DIAGNOSIS OF BREAST CANCER

Breast ultrasound is used as a complementary examination to mammography in the following situations; evaluation of dense breast tissues, evaluation of a mass demonstrated on mammography and guidance of biopsy procedures. The breast tissue is examined by very high frequency transducer ($\sim 10MHZ$). The basic principle of US is that the amplitude of the echo generated by the ultrasound reflections at an interface depends on the difference in the acoustic impedance between the two tissues. Example fat/dense connective tissue is strongly echogenic

than fat/parenchyma interfaces or dense connective tissue/parenchymal interfaces. Fatty tissues appear on sonographs as low acoustic impedance and spare low- level echoes (hypoechoic) where by fibrous tissues are seen as high-level intensity echoes with relatively high acoustic impedance [39]. The skin and fibro-glandular structures are relatively echogenic while subcutaneous and retromammary fat layers are seen as hypoechoic.

Generally benign breast tumors are seen on sonographs as smooth or microlobulated masses with well-marinated borders. They are homogeneous, oval and wider than tall. They do not attenuate the ultrasound beam (thus have no posterior shadowing). They can, however, displace rather infiltrate surrounding tissue. Doppler evaluation is either negative or shows some peripheral flow [16]. Malignant breast tumors on the other hand are generally hypoechoic and inhomogeneous, often attenuate the ultrasound beam and also cause posterior shadowing. Malignant breast tumors on the other hand usually infiltrates tissues rather than displacing it and has a tall rather than wide formation [16]. They are generally speculated and have boarders which are poorly marinated or microlobulated [39]. Microclacifications maybe present and may or may not be detectable with ultrasound. Malignant tumors normally characterized with neovascularity so Doppler evaluation typically shows an increase in blood flow. More of these characteristics can be found in Table 3.2

US can reliably diagnose simple cysts (100% accuracy with experience radiographer) presented as palpable masses or as indeterminate, nonpalpable lesions on mammography [39]. Now due to the advancement in the US equipment and refinement of breast imaging techniques, detection and characterization of small lesions has improved although it sometimes fails to detect small, nonpalpable cancers and cancers smaller than 5mm within normal breast tissue [6]. US has a major limitation when it comes to the detection of microcalcifications which is crucial for the diagnosis of breast cancer. That is, microcalcifications are hardly visible on US. An example is those located inside echogenic and fibroglandular breast tissues which makes it difficult to distinguish them form the echogenic interfaces among tissues [6].

In needle biopsy, this limitation can lead to difficulty in locating the exact location of the calcifications detected on a mammography as shown in Fig.3.4. The lesion is nonpalpable and contains microcalcifications but when the same patient was diagnosed using US, the microcalcifications were not detected as can be seen in the figure at the right of Fig.3.4. During biopsy, placing of the needle can be difficult since these calcifications can not be seen on the ultrasound. In this case for instance, an alternative method need to be use, example core needle biopsy with stereotactic guidance or mammographically guided wire localization. Although

Table 3.3: *Ultrasound characteristics of benign and malignant tumors* [16]

Bengn tumors	Malignant tumors
No internal echoes	Irregular shape or spiculated outline
Posterior enhancement	Angular or greater than three lobulations
Homogeneous or hyperechogenicity	Microlobulated and ill-defined
Thin echogenic pseudocapsule	Spiculated margins
Around the lesion	Marked hypoechogenicity
Ellipsoid shaped (width greater than anterior-posterior diameter)	Anterior-to-posterior diameter (height)greater than width (taller than wide)
Fewer than four gentle lobulations	Attenuating distal echoes
More easy to compress than malignant lesions	Duct extension
Acoustic shadowing is even and less marked in benign lesion	punctuate calcifications

both techniques are successful for aiding in diagnosis , the techniques requires mammographic compression of the breast which is uncomfortable for the patient beside the exposure to ionizing radiation [40]. Thus these methods have some negative effect on the patient which makes it difficult or impossible for the patient to tolerate sometimes [40]. In general, patients prefer sonographically guided procedures to mammographically guided procedure due to the fact that they feel very comfortable, the breast is not compressed, its faster, needle insertion site is more flexible,the needle can also be observed in real time and finally,no exposure to ionizing radiation [40, 6].

3.3 ULTRASOUND PHANTOMS

Ultrasound phantoms were first described in the 1970s. It can be any structure that contains one or more materials that simulate a body of tissues in its interaction with ultrasound. Thus it is used to mimic ultrasonic interaction in the human

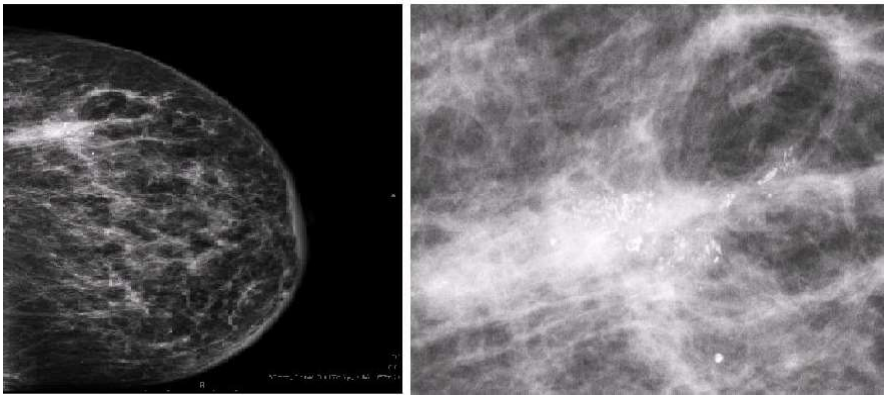

(a) *Mammogram*

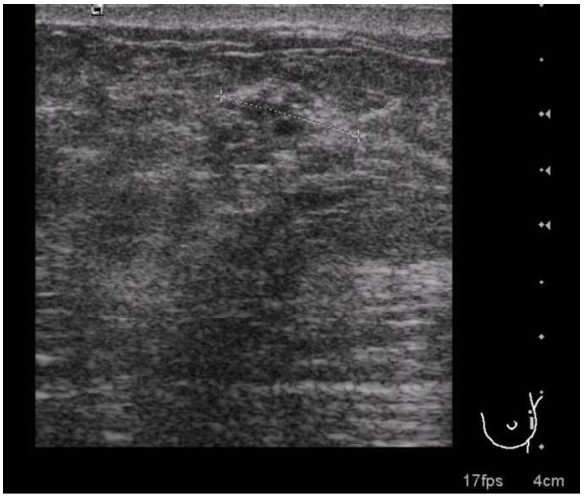

(b) *Ultrasound*

Figure 3.4: *Diagnosis of Breast cancer with mammogram and ultrasound: Microcalcifications detected on a mammogram (a) but not on ultrasound(b) [41].*

body. Phantoms can be used to check the performance of an ultrasound scanner by displaying and examining the images which it produces from the phantoms. They can have different geometry, scattering and absorbing characteristics, but it is generally of two types: those for simulating tissue and those for practicing biopsy producers. Tissue-like phantoms are meant to produce a B-scan appearance similar to the parenchyma of an organ, example liver (a finely textured echo pattern). These phantoms are used for testing and calibration of grey-scale ultrasound scanning equipment (thus important for quality control). They require a great effort in order to control factors like the speed of sound through the phantom, attenuation and scattering coefficients. They can also be time-consuming and expensive to produce. Biopsy phantoms on the other hand are developed just to represent the sonographic appearance of tissue for practicing biopsy procedures. With this, inexpensive materials can be used, so it is easy to make and are not so expensive. Thus phantoms are utilized for a variety of purposes such as training, quality control and demonstrations. An ultrasound phantom consists of tissue mimicking material, a target (what you want to image) and housing (phantom container).

Part II

MATERIALS AND METHOD

Chapter 4

PHANTOM MAKING

This chapter describes the phantom making process. The first section explains the procedure for making the phantoms and the various phantoms made (A - Æ and then Æ- D2). Detailed list of the materials, equipment, quantities of materials and chemicals used and then the final procedure used can be found at Appendix A. The last part of this chapter describes phantoms made for the detection of change in $\beta_n\kappa$.

4.1 PHANTOM MATERIALS

A tissue-mimicking material for ultrasound phantoms should have a very low acoustic backscatter coefficient about $40dB$ [42]. An ideal material is capable of mimicking soft tissue with respect to speed of sound, ultrasonic attenuation, and ultrasound scattering. The speed of sound in this material ranges from $1460 - 1640$ m/s and the attenuation coefficient from $0.4 - 0.7$dB/cm/MHz [42]. Also, its attenuation coefficient is proportional to the ultrasonic frequency [42]. Lastly, the material should be tough and robust to environmental fluctuations such as temperature, humidity etc. Examples of commercially available tissue mimicking materials are Zerdine, condensed-milk-based gel, urethane-rubber-based gel and a non-commercial agar-based gel. The attenuation coefficient and acoustic velocity of all these materials vary with temperature, but it is only agar which has a linear increase of attenuation with frequency [42]. The rest exhibits nonlinear responses of attenuation to frequency with varying degrees. Also, Zerdines, urethane and agar have attenuation coefficients of $0.5dB/cm/MHz$, but that of condensed milk is $0.5 - 0.7dB/cm/MHz$ [42].

In order to get accurate speed of sound and scattering in the phantom, a wide range of different substances may be added to the tissue mimicking material, example ethanol, n-propanol, glycerol etc. Ethanol and n-propanol have low boiling points, but glycerol is more convenient to work with and it also gives acoustics speed of $1537m/s$ [43]. Different inorganic particles can be used as scattering particles and attenuation regulation. Example of such particles are chalk, tale, graphite, carbon, grinding powder such as silicium carbide (can attain homogeneous scattering with well defined particle size of $8 - 12\mu$) and sephadex (A bead-formed gel prepared by crosslinking dextran with epichlorohydrin) etc. To prevent bacterial growth, benzoic acid can be used in addition to these chemicals.

4.1.1 Materials and Chemicals used for Making the Phantoms

The method used for making these phantoms was based on procedures described by Fredfeldt [43] and previous experiment done by Hilde [44]. In oder to meet experimental goals, the following materials and chemicals were used:

- Agar- based gel as bulk substance, that is, to mimic tissue. This was used because of it availability, low attenuation and is robust to temperature, humidity etc.
- Silicium carbide (SiC) of size $8.3 - 10.3\mu m$ for homogeneous background scattering.
- Sephadex of different sizes ($20 - 50\mu m$, $20 - 80\mu m$ and $50 - 150\mu m$) for homogeneous and adequate background scattering.
- Glycerol for adequate speed of sound.
- Distilled water for making up the total volume to $150ml$.
- Calcium particle of size $100\mu m$ and $190\mu m$ for imaging.
- Benzoic acid of concentration 0.022 M used to prevent bacterial growth. Thus when added to phantoms it can be used for a long time without any bacterials growing in the agar since agar is a good medium for bacterial growth.

More information about the materials, (quantities used for each phantom) and the equipment used can be found at Appendix A.1 and A.2

4.2 PROCEDURE FOR MAKING ALL PHANTOMS

The main procedure used for making all the phantoms can be summarized as seen in the block diagram at Fig.4.1 but a more precise one can be found at Appendix A.3. There were some slight variations in the materials used, for instance, benzoic acid was not used all the time due to availability at the start of experiment and also for checking errors. All phantoms without benzoic acid contains $135ml$ of distilled water. Secondly, in order to have adequate scattering which can make the calcium particles invisible by the conventional ultrasound as what is found in human tissues; the type, size and amount of scatterers were changed from time to time. The procedure was varied a bit when air bubbles were found at the layer where the calcium particles were placed in order not to confuse air bubbles with calcium particles in the ultrasound image. A total of 31 phantoms (A - Æ - D2) were made based on alterations or variations of materials (or chemicals) for the detection of the calcium particles together with 3 others phantoms (P - P2) for the detection of $\beta_n\kappa$. The various changes made are summarized as follows ;

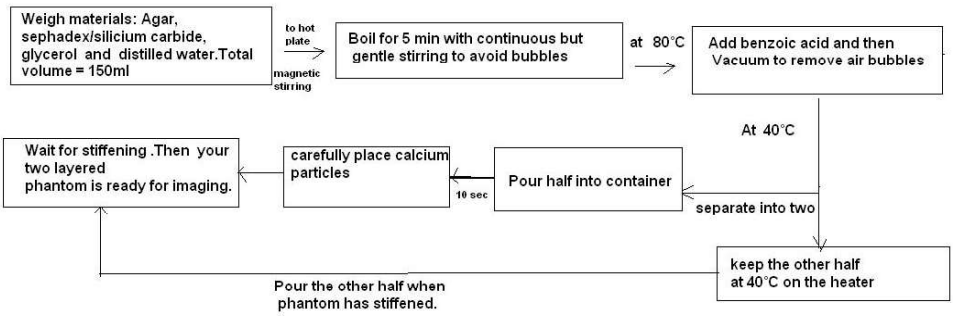

Figure 4.1: *Systematic steps for making an ultrasound phantom.* ***Note****: SiC was added at the same time time as benzioc acid due to the fact that sephadex forms clumps when added at* $80°C$.

4.2.1 Phantom A-C

These phantoms have the same recipe like that of Hilde's report (phantom W) [44]. Phantoms contains no benzoic acid and calcium particles due to availability. Vacuum was added from the beginning even before the solution began to boil, SiC was added too late and also the phantom was poured into the container too late, that is, $35°C$. Some adjustments were also made on the amount of scatterers

(SiC from $4.8672g$ to $5.0904g$) to get adequate scattering. See Table A.1 for more information on phantom A - C.

4.2.2 Phantom D-F

These phantoms contains benzoic acid and $190\mu m$ calcium particles. The amount of scatterers was change from $5.0904g$ to $6.5375g$ in order to make the particle invisible by conventional ultrasound. Thus comparable to what is found in human tissues.

4.2.3 Phantom G-J

Phantom G and H were made to investigate the cause of the air bubbles. In order to see the effect of benzoic acid, no benzoic acid was added to H (135ml of distilled water was used instead). Also in I, the solution was separated at $40°C$ but the second layer was added at $41°C$ whereby in J the separation was done immediately after SiC and benzoic acid were added to the phantom solution and a homogeneous solutions was obtained.

4.2.4 Phantom K-O

These phantoms contains the same amount of SiC. A lot of variations were done to in order to overcome the problem of bubbles. Some of these variations were; boiling the solution for 5 mins before cooling, avoiding shaking, minimum stirring and finally adding vacuum just after boiling. No calcium particles were placed in Phantom K and L, unlike M, N and O where particles were placed using magnifying glasses so as to know the exact number placed and also the exact position. Phantom M contains 8 calcium particles ($190\mu m$) whereby O contains $\sim$ 20 calcium particles ($190\mu m$) but the number of particles in N is unknown since it was difficult to count them. They all contain benzoic acid expect K. Also, the same procedure was used for all except L and M which were made just as J. Phantom L was poured into container too late $38°C$. See Fig.5.1

4.2.5 Phantom P and Q

In these phantoms, the amount of SiC was increased to $13g$ but the same procedure (as described above) was used. Phantom P has 8 particles of size $190\mu m$ where Q contains $\sim$ 20 calcium particles ($100\mu m$).

4.2.6 Phantom R and S

Phantoms R and S were made just to check the scattering properties of the sephadex. No benzoic acid was added to any of these phantoms. More information on the quantities used can be found in Table A.2.

4.2.7 Phantom T-V

Phantom T, U and V were made from three different sizes of sephadex, that is, $50-150\mu m$, $20-80\mu m$ and $20-50\mu m$ respectively to check the size of sephadex that gives adequate scattering. Eight calcium particles (seven in the middle and one at the side) were place in phantom T, six (at the side because air bubbles were found in the middle) were placed in U and eight were placed in V, that is, six in the middle and two at the side. The size of the calcium particles used for all phantoms was $190\mu m$.

4.2.8 Phantom W-Æ

In order to know the exact amount of sephadex that could make the calcium particles invisible by the conventional ultrasound as in real cases, these phantoms were made with twice as much sephadex as in phantom T-V. Phantom W and Z contains sephadex of size $50-150\mu m$ and $190\mu m$ calcium particles. The size of sephadex in phantom X, Y and Æ is $20-80\mu m$. Phantom X contains six $190\mu m$ calcium particles in the middle whereby Y contains ~ 50 of $100\mu m$(hard to place the particles even though magnifying glasses were used) particles but no calcium particles were placed in Æ, that is, used as reference phantom. See Appendix A.3 and Table A.2 for more information.

4.2.9 Phantom A2 - D2

The same amount ($8g$) and size of sephadex ($20-80\mu m$) was used except D2 which contains 14g but contains the same size of sephadex. Phantom B2 was used as a reference so no calcium particles were placed inside, A2 and D2 contains 8 calcium particles ($190\mu m$) placed in the middle as shown in Fig.4.2. C2 contains ~ 40 calcium particles of size $100\mu m$. More information can be found in Table A.2. See Fig.5.1 for phantom A2.

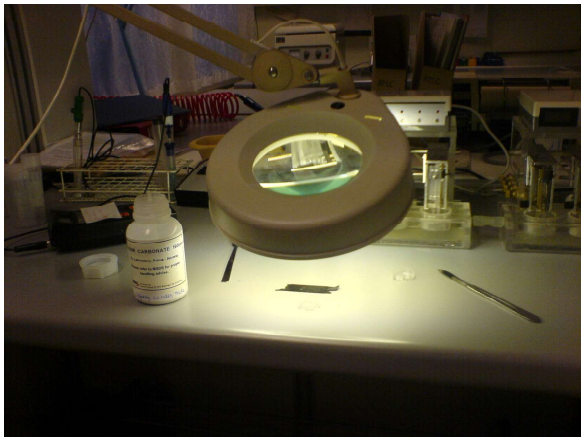

(a)

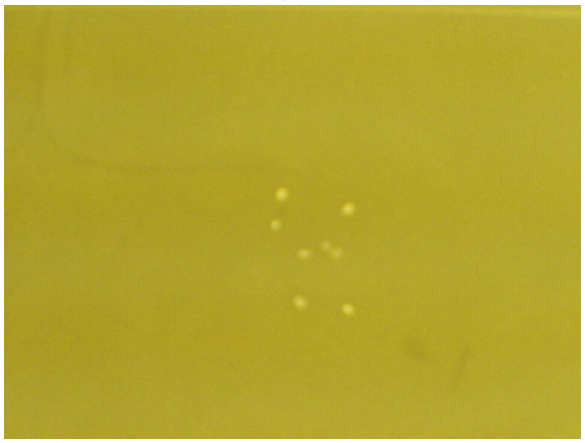

(b)

Figure 4.2: *(a) Magnifying glass for placing particles in phantoms. (b) Calcium particles placed in the center of phantom*

4.2.10 Propagation phantoms P

Two phantoms with different concentrations of glycerol (10% and 20%) were made for the detection of $\beta_n\kappa$. The same recipe was used for P1 and P2 but no calcium particles were placed inside. Also P1 contains 10% of glycerol whereby P2 contains 20% of glycerol as seen in Table A.3. The two layered phantom on the other hand contains half amount of the materials used in P1 and P2. Thus the bottom contains 10% of glycerol (same concentration as P1) and the top 20% (same concentration as P2) but the same procedure was used in making these phantoms as well. See Table A.3 for more information.

4.3 LAB EQUIPMENT

Detailed list of the equipment used in making the phantom can be found at Appendix A.1.

4.3.1 Ultrasound Equipment used for Imaging Phantoms

The phantoms were imaged with a conventional ultrasound scanner (Vivid 7) from Vingmed. An M12L probe was used for imaging all phantoms and the application used is called small parts. For consistency, the same settings were used for imaging all phantoms. Images were taken from the side of the phantoms as well as from the top (when the phantom was flat). Fig.4.3 shows an image of how the phantoms were imaged from the side.

According to the aim of the project, the phantoms were to be imaged with the SURF method but due to some problems with the equipment (noise in the received signal when used for imaging) it could not be done as intended.

4.3.2 Mammography

In order to show that the calcium particles were placed in the phantoms, phantoms were also imaged with mammogramphy from "Mammografiavdeling" (Avdeling for bildediagnostikk) at the ST.Olav's hospital. The name of the mammogram is called Senographe DS acquisition system from GE healthcare. All phantoms were imaged from the side and then from the top as in the ultrasound but different settings were used, unlike the ultrasound. For phantoms made with silicium carbide, these

Figure 4.3: *Phantom Imaged from the side with Vivid 7 scanner (M12L probe).*

settings were used; LCC or LMCC, Dose: 1.2–8.1 mGy, voltage: 27–29 kV, current: 56–100 mAs. Phantoms from sephadex were however imaged with these settings; LMCC or LMXCCM, Dose: 7.5–9.7 mGy, voltage: 29–32 kV, current: 100–125 mAs.

Part III

RESULTS

Chapter 5

RESULTS

This chapter summaries the characterization (results) of all phantoms that were made.

Generally, phantoms K, M, O, A2, B2, C2 and the propagation phantoms were found to be good but the rest can not be because they contain a lot of air bubble, clumps and inadequate amount of scatterers. That is, due to lack of experience there were lot of air bubbles on the layer where the calcium particles were placed which makes it difficult to distinguish them (air bubbles) from the calcium particle in the sonograph as can be seen in Fig.5.2. See Fig. 5.1 for samples of phantoms from silicum carbide and sephadex.

All phantoms imaged with both the mammogram (Senographe DS acquisition system) and ultrasound (vivid 7) have equal dimensions since the containers used are of equal dimensions. Images were taken from the top and then from the side but the calcium particles were more visible when imaged from the side than from the top of the phantom. Images taken with the mammogram, however shows particles much more visible from the top than from the side.

5.1 PHANTOMS MADE FROM SILICIUM CARBIDE

The results from all phantoms made with silicium carbide has been summarized in Table B.1 at Appendix B. Phantoms A-Q were not as good as phantoms K, M and O since they were full of air bubbles and clumps. This shows that air bubbles must be done away with, at least at the layer where the calcium particles were placed. Phantoms K, M, and O were good since no air bubbles were found in the phantom especially at the layer where the particles were placed. These three

phantoms contain approximately the same amount of silicium carbide ($6.6g$) of size $8.3-10.3$ as can be seen in Table A.1. They (phantoms K, M, and O) also have

Figure 5.1: *Phantoms made with silicium carbide (left) and sephadex (right).*

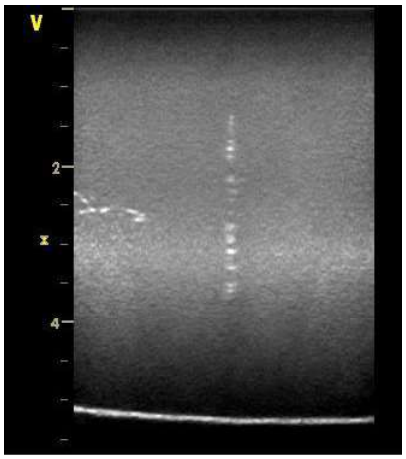

Figure 5.2: *Sonograph of Phantom F; air bubbles found at the left side and at the layer where calcium particles were placed. Diffcult to distinguish air bubbles from calcium particles.*

homogeneous scattering background as shown in Fig. 5.3 although the scattering was not adequate to make calcium particles invisible on the convention ultrasound as found in human tissues. See Fig. 5.4.

5.1.1 Phantom K

Phantom K is a reference phantom and so no calcium particles were placed inside the phantom. It was made to check the background scattering as can be seen from Fig.5.3, the image from both ultrasound and mammogram show homogeneous background. The mammography image of phantom K was taken with these settings; LCC, Dose: $1.2mGy, 29kV, 63mAs$ (from side) and LCC, Dose: $1.3mGy, 27kV 56mAs$ (from top).

5.1.2 Phantom M

Phantom M contains 8 calcium particles of size $190\mu m$. All the 8 calcium particles placed in the middle of the phantom were visible both on the ultrasound and the mammogram as shown in Fig. 5.4. The mammography image of phantom M was taken with these settings; LCC, Dose: $3.2mGy, 29kV, 63mAs$ (from side) and LCC, Dose: $3.5mGy, 27kV, 56mAs$ (from top).

5.1.3 Phantom O

The phantom contains $\sim$ 20 of $100\mu m$ calcium particles. The particles were a bit more visible on the ultrasound image from the side than the one from the top and also it was hard to see on the mammography. See Fig.5.5. The mammography image of phantom O was taken with these settings; LMCC, Dose: $3.2mGy, 29kV, 63mAs$ (from side) and LMCC, Dose: $8.1mGy, 29kV, 100mAs$ (from top).

5.2 PHANTOMS MADE FROM SEPHADEX

The results from all phantoms made with sephadex has been summarized in Table B.2 in Appendix B. Phantoms A2, B2, and C2 were good since no air bubbles were found in the phantom especially at the layer where the particles were placed. Phantoms R–Æ were not as good as A2–C2 although a homogeneous background

was obtained. This is because phantoms (A2, B2, and C2) have homogeneous back-

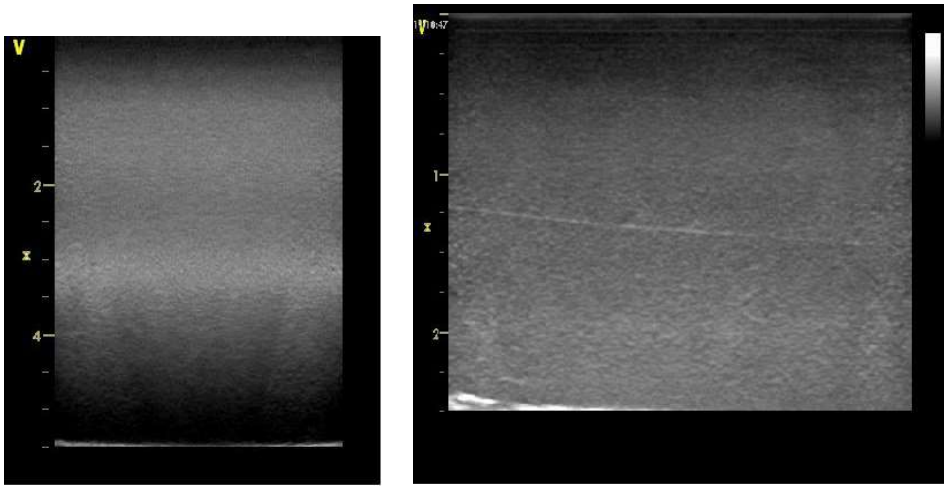

(a) *from side* (b) *from top*

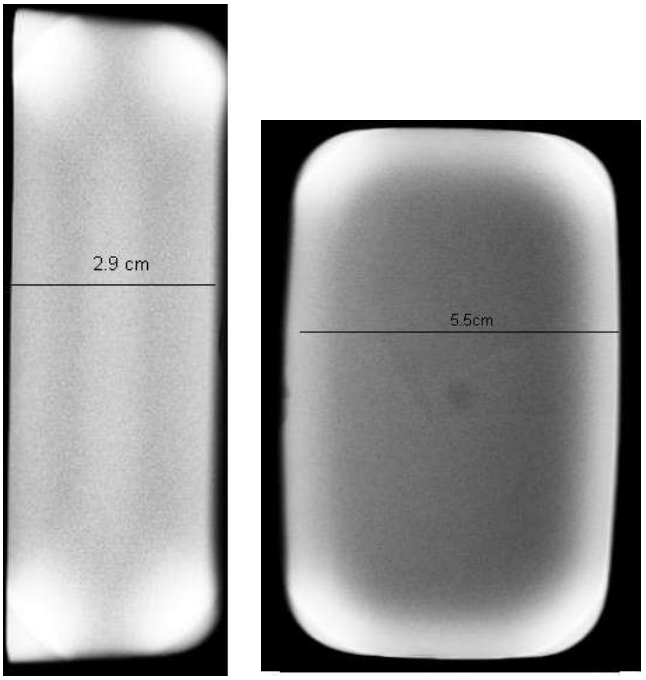

(c) *from side* (d) *from top*

Figure 5.3: *Sonograph ((a) and (b)) and mammogram ((c)and (d)) of Phantom K (reference phantom) without calcium particles imaged from the side ((a) and (c)) and from the top ((b) and (d)) of phantom. The amount of SiC used was (* $6.6g$*) with size* $8.3 - 10.3\mu m$

.

ground scattering which is adequate enough to make particles quite invisible on the conventional ultrasound comparable to what is found in normal breast tissues. These phantoms (A2–C2) contain approximately the same amount of sephadex

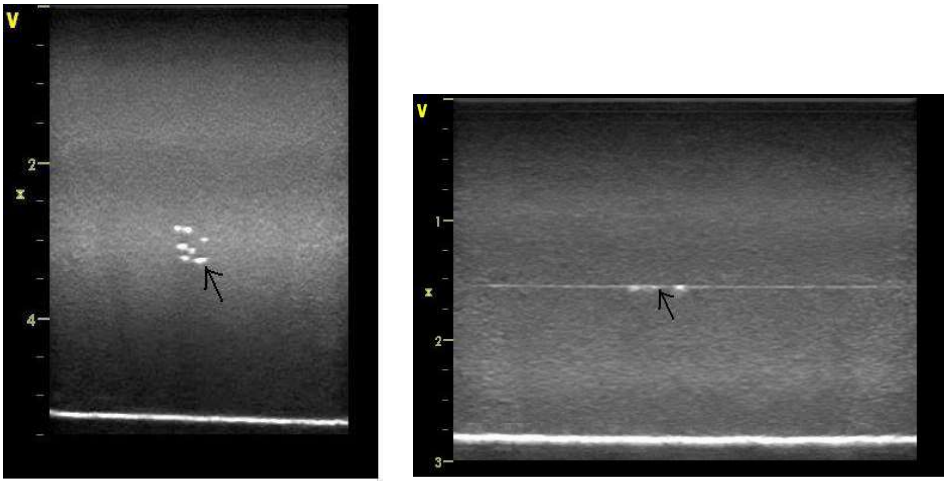

(a) *from side* (b) *from top*

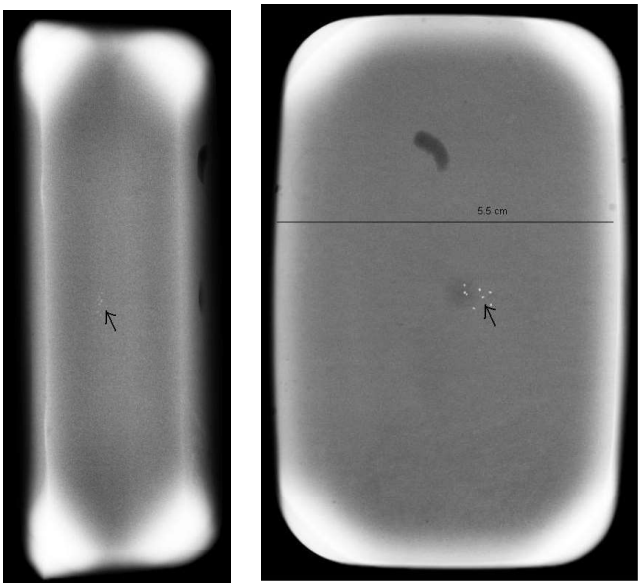

(c) *from side* (d) *from top*

Figure 5.4: *Sonograph ((a) and (b)) and mammogram ((c)and (d)) of Phantom M imaged from the side ((a) and (c)) and from the top ((b) and (d)) of phantom. All the 8 calcium particles of size* $190\mu m$ *(black arrow) placed in the middle of the phantom were visible both on the ultrasound and the mammogram. The amount of SiC used was (* $6.6g$*) with size* $8.3 - 10.3\mu m$

.

($\sim 8g$) of size $20 - 80\mu m$ as can be seen in Table A.2. No distinct layer was seen on the sonographs (ultrasound images of A2, B2,and C2) as seen in the case of Silicium carbide.

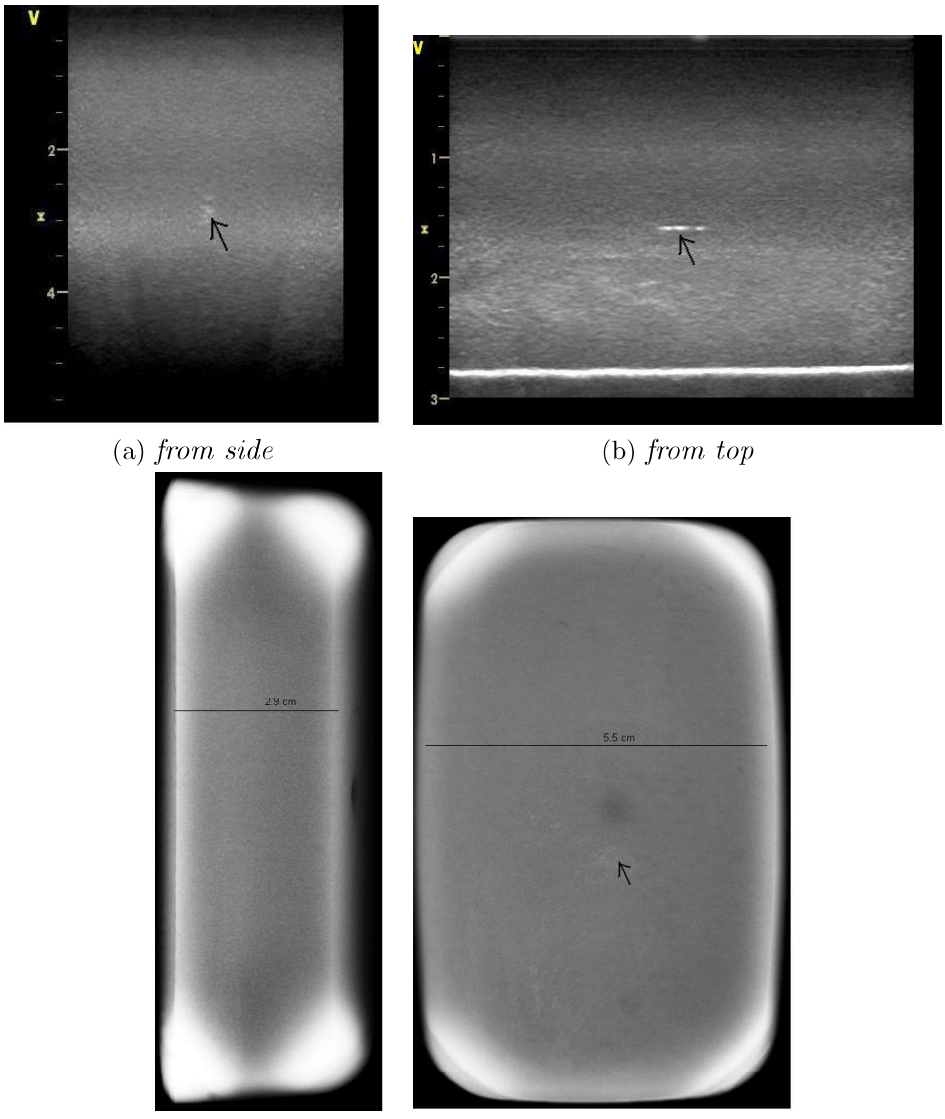

(a) *from side* (b) *from top*

(c) *from side* (d) *from top*

Figure 5.5: *Sonograph ((a) and (b)) and mammogram ((c)and (d)) of Phantom O imaged from the side ((a) and (c)) and from the top ((b) and (d)) of phantom. The amount of SiC used was (* $6.6g$*) with size* $8.3 - 10.3\mu m$*). The calcium particles (*~ 20*) of size* $100\mu m$ *were much more visible on the sonograph than on the mammogram although it was hard to see particles (black arrow) in both cases especially (c).*

5.2.1 Phantom B2

Phantom B2 is the reference and it contains no calcium particles. It shows a homogeneous background both in the ultrasound and the mammogram image. See Fig:5.6. The mammography image of phantom B2 was taken with these settings; LMCC, Dose: $9.3mGy, 32kV, 125mAs$ (from side) and LMXCCM, Dose: $8.7mGy, 30kV, 100mAs$ (from top).

5.2.2 Phantom A2

Phantom A2 contains 8 calcium particles of size $190\mu m$. All the eight calcium particles ($190\mu m$) placed in the middle of the phantom were visible both on the ultrasound and the mammogram but were not as visible as seen in the case of silicium carbide. See Fig.5.7. The mammography image of phantom A2 was taken with these settings; LMCC, Dose: $9.7dGy, 32kV, 125mAs$ (from side) and LMCC, Dose: $8.4dGy, 30kV, 100mAs$ (from top) .

5.2.3 Phantom C2

This phantom contains 40 of $100\mu m$ calcium particles. For this phantom, the particles were not visible in the ultrasound or mammography image. See Fig.5.8. It looks like nothing was placed there just like the reference phantom. The mammography image of phantom A2 was taken with these settings; LMCC, Dose: $7.5mGy, 30kV, 125mAs$ (from side) and LMCC, Dose: $7.6mGy, 29kV, 100mAs$ (from top).

5.3 PROPAGATION PHANTOM

The speed of sound in phantoms were measured using the same probe as used for the detection of the calcium particles. The method used was not so accurate but some approximate valves were obtained as can be seen in Table 5.1. The same probe (M12L) was used to calibrate the length of the two phantoms and a ruler was then used to measure the actual length and then the speed of sound in the phantoms were calculated from Eq.5.1 below. The measurement was done with P1 and P2 since it was much easier to measure than the two layer (layer not visible).

$$\frac{l_m}{l_s} = \frac{c_m}{c_s} \tag{5.1}$$

$$\Rightarrow c_m = c_s \frac{l_m}{l_s} \tag{5.2}$$

where; l_m is the actual length measured with the ruler and c_m is the actual speed

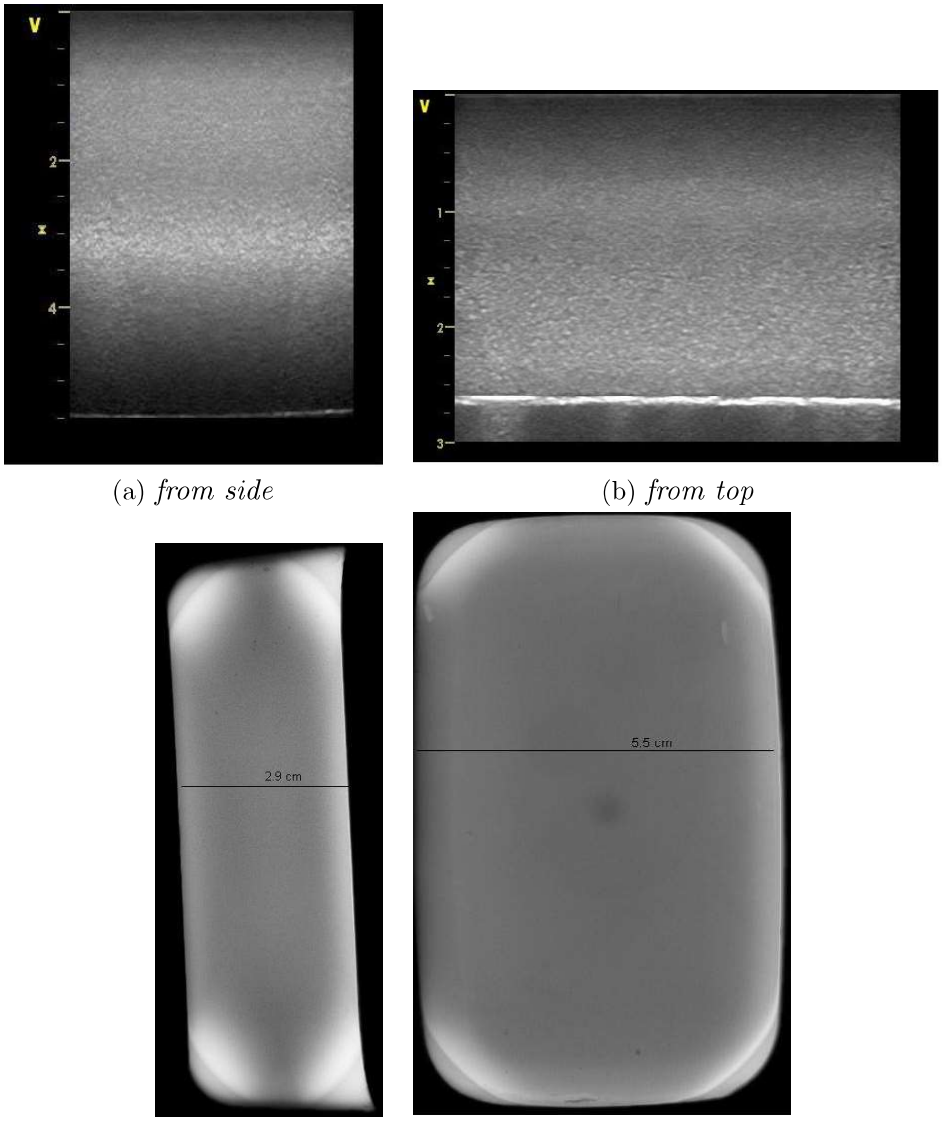

(a) *from side* (b) *from top*

(c) *from side* (d) *from top*

Figure 5.6: *Sonograph ((a) and (b)) and mammogram ((c)and (d)) of Phantom B2 (reference phantom) without calcium particles imaged from the side ((a) and (c)) and from the top ((b) and (d)) of phantom. The amount of sephadex used was (8g) with size* $20 - 80\mu m$

of sound measured. l_s is the length estimated by the scanner and c_s is the speed of sound estimated by the scanner which is $1540m/s$

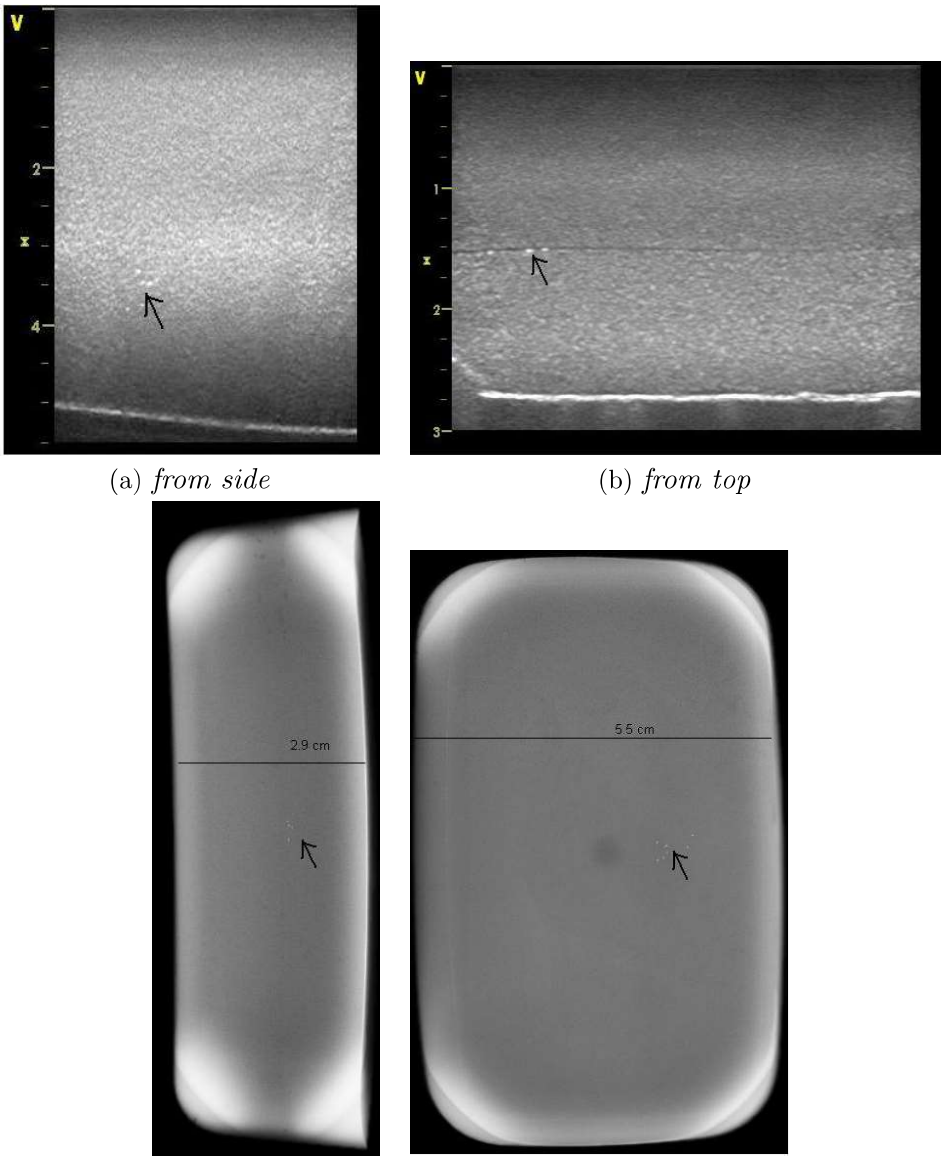

(a) *from side* (b) *from top*

(c) *from side* (d) *from top*

Figure 5.7: *Sonograph ((a) and (b)) and mammogram ((c)and (d)) of Phantom A2 imaged from the side ((a) and (c)) and from the top ((b) and (d)) of phantom. All the 8 calcium particles of size* $190\mu m$ *(black arrow) placed in the middle of the phantom were visible on both ultrasound and mammogram. The amount of sephadex used was (*$\sim 8g$*) with size* $20 - 80\mu m$

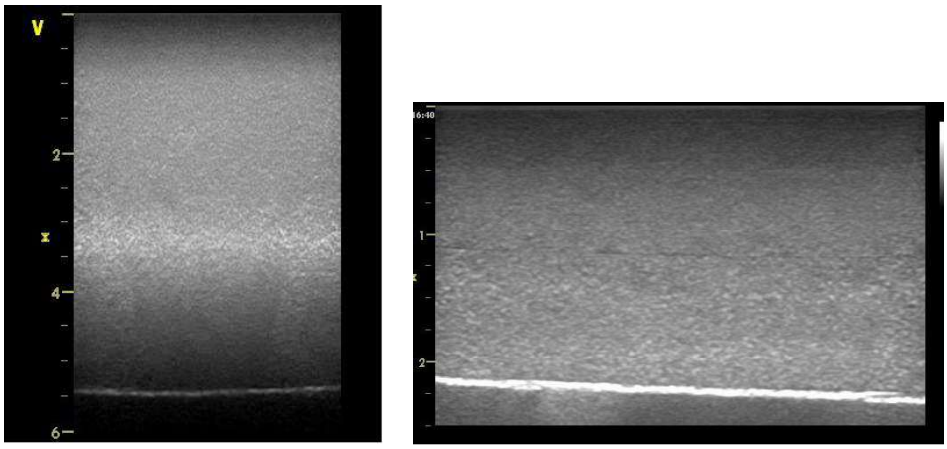

(a) *from side* (b) *from top*

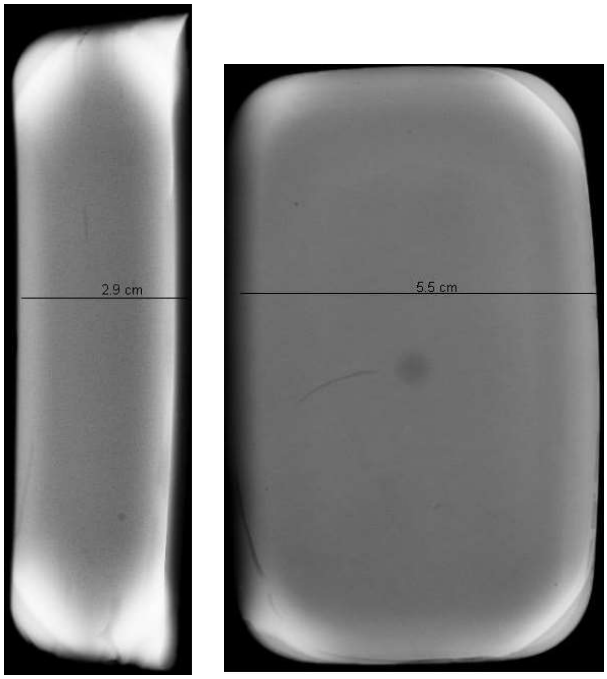

(c) *from side* (d) *from top*

Figure 5.8: *Sonograph ((a) and (b)) and mammogram ((c)and (d)) of Phantom C2 imaged from the side ((a) and (c)) and from the top ((b) and (d)) of phantom. The amount of sephadex used was (8g) with size* $20 - 80\mu m$*. The calcium particles* ~ 40 *of size* $100\mu m$ *were not visible in the sonograph or the mammogram (black arrow)*

.

Table 5.1: *Speed of sound in Phantom P1 and P2.*

Parameter	$l_s[cm]$	$l_m[cm]$	$c_s[m/s]$	$c_m[m/s]$
P1	4.67	5.05	1540	1665
P2	4.49	5.05	1540	1732

Part IV

DISCUSSION AND CONCLUSION

Chapter 6

DISCUSSION

In this chapter, the results obtained from the phantom making for the detection of microcalcfications and detection of $\beta_n\kappa$ is discussed in order to understand the impact and its implications. This was followed by how the SURF imaging can improve the diagnosis of breast cancer in the clinic.

Phantoms A-Q and R-Æ were not good and can not be used for the detection of microcalcifications because they contain air bubbles especially at the layer and so it difficult to distinguish air bubbles from calcium particle in the sonograph. See Table B.1 and B.2. Another reason is that most of them do not contain benzoic acid so they cannot be kept be for a long time. Generally, phantoms A2, B2, C2, P1 and P2 were found to be good and can be used for future experiments since they all contain benzoic acid and there are no air bubbles at the layer. The sonographs also show background scattering comparable to what is found in human tissues. As seen from the images, example Fig. 5.6, these phantoms have homogeneous background scattering which corresponds to procedures described by Hilde [44]. Phantom K, M, and O were also good and can be used for future experiments but the sonographs show inadequate background scattering although the background is homogeneous. This is because the scattering produce from SiC was not adequate to make the particles invisible on sonograph as what is found in real cases with human tissues.

Particles were more visible when imaged from the side than from the top due to the layer in the phantom. Thus all the particles lie in the same plane when viewed from above but when viewed from the side they appear as individual ones. This can be explained by the fact that ultrasound images with depth. In mammopraph the opposite is true. See Fig. 5.4 and 5.7.

6.0.1 Phantoms made with Silicium Carbide

Homogeneous scattering was obtained with 5% concentration ($\sim 5g$) which correspond to procedures described by Fredfeldt [43] but was not adequate for making the the calcium particles invisible by conventional ultrasound. See Fig.5.4. This is because the size of the scatterers (SiC) is much smaller ($8.3 - 10.3\mu m$) than the wavelength of ultrasound used ($\sim 128\mu m$) so it produces very little scattering. From Table A.1 it can be seen that the highest amount of silicium carbide used (Phantom P and Q) was $\sim 13g$ which is more than 10% concentration. According to the procedure described by Fredfeldt [43], a particle size of $8 - 12\mu m$ with 5% concentration is enough for obtaining homogeneous scattering with attenuation of $0.4dB/MHz$ with a frequency of 4MHz. It was also observed that as the amount of scatterers was increasing the attenuation also increases. This might be as a result of the high frequency used in this experiment, that is, $\sim 12MHz$. Also it becomes more difficult to stir as the amount of SiC was increased and this would have resulted in heterogenous phantoms.

The implication of this is that, the whole depth of the phantom cannot be imaged or seen since the waves are attenuated and so it is difficult to tell whether there are particles or not. Also, the $100\mu m$ particles were more visible on the ultrasound image than the mammography although mammography is more sensitive than ultrasound when it comes to the detection of microcalcifications [6]. This is because the phantoms have homogeneous background unlike what is found in human tissues which makes it easier for the ultrasound to detect the particles . Mammogram can detect microcalcifications found in the breast down to $0.2 - 0.3mm$ [15] whereby the microcalcifications associated with breast cancer are $\leq 0.5mm$ in size [15]. This implies that mammography is less sensitive when the calcifications are much smaller.

6.0.2 Phantoms made from Sephadex

These phantoms gave better results than the ones made from silicium carbide. They have a homogeneous background scattering and also the scattering was adequate to make the calcium particles invisible with an amount of $8g$. Although the calcium particles can be seen both by ultrasound and mammography, they were not as visible as in the case of the silicium carbide. See Fig. 5.7. This is as a result of the size of the sephadex used ($20 - 80\mu m$) which is bigger than that of the silicium carbide and not so small compared to the wavelength of Ultrasound. As seen in Fig. 5.8, the $100\mu m$ particles were not visible both by ultrasound or mammography because the scattering produced by sephadex was adequate to make

them invisible by the conventional ultrasound comparable to human tissues. The implication is that, the mammogram and the ultrasound are not sensitive enough when the particles are so small which confirms earlier work done by Kopans [15] and Nagashima [6]. Finally no distinct layer was seen in the image as compare to SiC phantoms because the sephadex was able to produce sufficient scattering to hide the layer. Again the reason being the difference in size. See Fig. 5.4 and 5.7.

6.1 PROPAGATION PHANTOMS

From Table 5.1 it can be seen that the speed of sound in the phantom with 10% and 20% glycerol ($1665m/s$) was a bit higher as compare to the procedure described by Hidle [44]. This might be due to the inadequate method used in the estimation. Hopefully more accurate values would be obtained when the correct procedures are used and also when the SURF imaging is used in testing. These phantoms can be used to detect the change in $\beta_n\kappa$ which can be useful in tissue characterization for the diagnosis of cancer.

6.2 SURF IMAGING FOR DIAGNOSING BREAST CANCER IN THE CLINIC

As said earlier on in the introduction, breast cancer is the most common cause of cancer death in women worldwide and the mortality rate can be reduced by early detection because it increases the chances of successful treatment. Most breast carcinomas exhibit clustered microcalcifications which is an essential feature in terms of breast cancer diagnosis. Also nonpalpable and pre-cancerous carcinomas can be diagnosed best by the detection of microcalcifications, example DCIS and LCIS, which means that the detection of microcalcifications is crucial for breast cancer diagnosis.

Although mammography is sensitive for the detection of microcalcifications, the patient is exposed to ionizing radiation unlike ultrasound. As discussed in Section 3.2, ultrasound has a major limitation when it comes to the detection of microcalcifications which is crucial for the diagnosis of breast cancer. That is, microcalcifications are hardly visible by conventional ultrasound. An example is calcifications located inside echogenic and fibroglandular breast tissues which makes it difficult to distinguish them from the echogenic interfaces between tissues [6]. Also there is an overlap in the sonographic appearance of benign and malignant masses [15]

which makes it difficult for the physician to solely rely on breast ultrasound to avoid biopsy procedures.

This limitation can be overcome by using SURF imaging. It has not been proved experimentally, however, it can be seen from Section 3.1.2 that the use of SURF imaging can improve the contrast between the microcalcifications and that of the breast tissue with a contrast ratio of $\sim 14dB$ when the linear scattered signal is suppressed by least -34dB [9].

The implication is that with SURF imaging;

1. Detection of microcalcifications can be done more precisely since there is better contrast and this will limit the number of biopsy procedures and surgery. Also, the patient will not be exposed to ionizing radiation and will be free from the trauma of surgery or biopsy.

2. Distinguishing between benign and malignant masses will be more accurate due to the increased contrast and by the estimation of $\beta_n\kappa$ for tissue characterization.

3. One can obtain improved image quality are obtained.

4. Detection of ultrasound contrast agents will be substantial improved compared to that of conventional ultrasound.

Chapter 7

CONCLUSION

This report describes how SURF imaging (dual-frequency technique) can be used to improve the detection of microcalcifications by ultrasound for breast cancer diagnosis. SURF is based on transmission of two different pulse complexes (a high and a low frequency pulse as shown in Fig.3.1). The high frequency is used for imaging whereby the low frequency is for manipulating the acoustical backscattering and propagation properties of the high frequency pulse (imaging pulse).

In conclusion, ninety percent of all breast tumors starts from the lobules and the ductsof the breast (carcinomas) where by the rest starts from the stroma (sarcomas) tissues of the breast. The two main types of breast cancer are ductal carcinoma and lobular carcinoma. Also 90% of all breast cancers is ductal carcinoma. Clustered microcalcifications is a common feature of tumors found in the breast (asymptomatic and symptomatic cancer) and so detection of microcalcifications is crucial for early breast cancer diagnosis in order to reduce the mortality rate of breast cancer.

SURF imaging can provide an increased contrast between the calcifications and the breast tissues by suppressing the linearly scattered signal from the tissues by -34 dB. Thus with SURF imaging, one can get a contrast ratio of nonlinear microcalcification scattering and nonlinear tissue scattering to be $\sim 14dB$. One can then accurately distinguish malignant tumors from those of benign and this can reduce the number of biopsy procedures, surgery and mammography.

Although the aim of the project was to demonstrate the detection of microcalcifications by SURF imaging, unfortunately the phantoms were not imaged or tested with SURF imaging, due to problems with the equipment as stated earlier on in Section 4.3.1. From the results obtained from phantom making, it can be concluded that phantoms have been made for the detection of microcalcifications

which are good and can be used for future experiments. The $190\mu m$ calcium particles were visible both by the ultrasound and mammography for the different types of scatterers used (SiC and sephadex). However, the $100\mu m$ calcium particles were not visible by neither mammography nor ultrasound when sephadex was used as scatterers. Nevertheless they were visible on the conventional ultrasound and a bit visible by mammography when silicium carbide was used. Phantoms for detecting the change in $\beta_n\kappa$ were also made and the speed of sound was determined to be 1665 m/s for phantom with 10% of glycerol and $1732m/s$ for phantom with 20% of glycerol.

Future Work

As can be seen this project need to be continued to achieve the full aim. The following are some of the things that need to be done to fully achieve the aim of the project.

1. Image the phantoms containing calcium particles with SURF imaging to see if it is possible to detect the particles with increased contrast.
2. Image the two phantoms with different concentrations of glycerol to estimate the speed of sound in each and check if it is possible to detect the change in $\beta_n\kappa$. Thus more accurate method can be used to measure the speed of sound in these phantoms.
3. Further into the future, clinical trials can be done to see if is it possible to detect microcalifications for the diagnosis of breast cancer.

Part V

APPENDICES

Appendix A

DETAILS ON PHANTOM MAKING

A.1 LIST OF EQUIPMENT AND CHEMICALS USED IN MAKING AN IDEAL PHANTOM

A.1.1 List of Equipment

- One hot plate
- three magnetic stirrer(one with hot plate two without hot plate).
- Magnets for stirring.
- Scale balance for weighing.
- Spoons.
- 3 conical flasks of size 250ml.
- Lab coat and gloves.
- 2 measuring cylinders of size 100ml.
- 3 measuring cylinders of size 25ml.
- Pipettes.
- Thermometer.

- Plastic containers for phantom.
- Parafilm used to cover phantoms.
- Refrigerator for storing phantoms.
- Ultrasound scanner (Vivid 7 from Vingmed) for imaging *i.e.* M12L probe.
- Mammography from "Mammografiavdeling" (Avdeling for bildediagnostikk) at the ST.Olav's hospital.

A.1.2 List of Chemicals

- Agar- based gel as the bulk substance. From Apotek produckjon AS Oslo - Norway.
- Silicium carbide (SiC) of size $8.3 - 10.3\mu m$. From MSDS
- Sephadex of size $20 - 50\mu m$, $20 - 80\mu$ m and $50 - 150\mu m$. From Amersham Biosciences limited - Sweden (MSDS).
- Glycerol for adequate speed of sound. From Proalanlys Merck KGaA Darmstadt - Germany.
- Distilled water for making up the total volume.
- Calcium particle of size $100\mu m$ and $190\mu m$. From MISWACO M - I Norge AS Stavanger (MSDS)
- Benzoic acid of concentration 0.022 M. From Merck KGaA Darmstadt - Germany.

A.2 SUMMARY OF ALL PHANTOMS MADE

Table A.1: *Summary of all phantoms made with silicium carbide (8.3-10.3 μm) as a scattering material. Number of* 190μm *calcium particles indicated but only approximate values were given to the number of* 100μm *particles because it was hard to count them.*

Phantom	**Agar** $[g]$	**Silicium-carbide**$[g]$	**Glycerol** $[ml]$	**Distilled water**$[ml]$	**Benzoic acid (0.022** M**)**$[ml]$	μ**Ca** $/[\mu m]$
A	3.7392	4.8715	15	135	-	-
B	3.7382	4.8672	15	135	-	-
C	3.7378	5.0904	15	135	-	-
D	3.7382	6.5375	15	110	25	?/190
E	3.7332	6.5048	15	110	25	?/190
F	3.7442	6.5559	15	110	25	?/190
G	3.7343	6.5552	15	110	25	-
H	3.7376	6.5174	15	135	-	-
I	3.7516	6.5056	15	135	-	7/190
J	3.7360	6.5308	15	110	25	-
K	3.7305	6.5228	15	135	-	-
L	3.7497	6.5391	15	110	25	-
M	3.7306	6.5849	15	110	25	8/190
N	3.7386	6.5607	15	110	25	?/190
O	3.7367	6.5588	15	110	25	∼20/100
P	3.7331	13.0618	15	110	25	8/190
Q	3.7396	13.0116	15	110	25	∼20/100

Table A.2: *Summary of all phantoms made with sephadex as a scattering material. Number of* $190\mu m$ *calcium particles indicated but only approximate values were given to the number of* $100\mu m$ *calcium particles because it was hard to count them.*

Phantom	**Agar** $[g]$	**Sephadex** $[g]/[\mu m]$	**Glycerol** $[ml]$	**Distilled water**$[ml]$	**Benzoic acid (0.022** M**)**$[ml]$	μ**Ca solid/**$[\mu m]$
R	3.7325	0.8423/-	15	135	-	-
S	2.4923	0.4369/-	10	90	-	-
T	3.7461	1.0187/ 50-150	15	110	25	8/190
U	3.7346	1.0159/ 20-80	15	110	25	6/190
V	3.7373	1.0465/ 20-50	15	110	25	8/190
W	3.7398	2.0794/ 50-150	15	110	25	5/190
X	3.7438	2.0972/ 20-80	15	110	25	6/190
Y	3.7325	2.0412/ 20-80	15	110	25	∼50/100
Z	3.7377	8.0135/ 50-150	15	110	25	8/190
Æ	3.7387	2.0825/ 20-80	15	110	25	-
A2	3.7372	8.0192/ 20-80	15	110	25	8/190
B2	3.7417	8.0153/ 20-80	15	110	25	-
C2	3.7359	8.0964/ 20-80	15	110	25	∼40/100
D2	3.7419	14.0029/ 20-80	15	110	25	8/190

Table A.3: summary of all phantoms made for the detection of $\beta_n\kappa$ with SURF Imaging

Phantom	**Agar** $[g]$	**Sephadex** $[g]/[\mu m]$	**Glycerol** $[ml]$	**Distilled water**$[ml]$	**Benzoic acid (0.022** M**)**$[ml]$
P1	3.7367	2.0854/20-80	15	110	25
P2	3.7394	2.0009/20-80	30	95	25
P, 1. two layer	1.8694	1.0772/20-80	7.5	55	12.5
P, 2. two layer	1.8692	1.0552/20-80	15	47.5	12.5

A.3 PROCEDURE FOR MAKING AN IDEAL PHANTOM

A.3.1 Benzoic Acid Soloution

- 0.5499g of benzoic acid was weighed into 250ml flask.
- Distilled water was then added to the make a total volume of 200ml thus a concentration of 0.022M.
- The solution was then boiled for 2mins on a hot plate with a magnetic stirrer but the bottle not completely closed to avoid high pressure inside the bottle.
- The bottle was opened any time it starts to bubble.
- The solution was transfered to the other magnetic stirrer when a homogeneous solution was obtained, that is, without any white particles.
- This solution was used for several (8) phantoms each with 25ml. The solution was kept at $25°C$ and was stirred prior to being used.

A.3.2 Phantom Solution

- $3.7325g$ of Agar and $8g$ of $20 - 80\mu m$ sephadex were then weighed into a 250ml conical flask. See Table A.2 for varying amount of materials.
- 15ml of glycerol and 110ml of distilled water were measured with the measuring cylinder and then added to the agar and sephadex in the flask to make a phantom solution. The flask was covered with a cork to avoid spurting.
- The mixture was put on a hot plate together with magnetic stirrer to boil for 5 min. In order to avoid air bubbles, stirring was set to low (number 5) but with continuous stirring. The bottle was opened as soon as the pressure is high.
- The phantom solution was then placed on a separate magnetic stirrer (without heating) for cooling. This time the stirrer was set to below number 5 (2-3) avoiding shaking to get rid of air bubbles.

A.3.3 Final Mix

- 25ml of benzoic acid was then added to the phantom solution at $80°C$ (due to its high boiling point) together with vacuum to remove the bubbles inside the phantom solution. *Note*: SiC was added together with the benzoic acid (when using SiC) but not at the same time as the agar.
- The temperature was checked from time to time since it start stiffening below $40°C$.
- Magnifying glasses were used to selectively pick the calcium particles to be placed on top of the first layer.
- At $40°C$ half of the solution was poured into a container (by using funnel in order to avoid air bubbles) while other half was kept at $40°C$.
- Calcium particles (either $100\mu m$ or $190\mu m$) were then placed at specific positions (thus a cluster was formed either at the middle or at the side) with a magnifying glasses after about 10 s. The solution was then allowed to cool or stiffen. The particles were normally placed in the center of the phantom for easy identification.
- The other half was added or poured (with a funnel) on top of the first layer after the solution has stiffen.
- The phantom was allowed to stiffen. A two layered phantom was formed and was kept in the refrigerator and then imaged the following day.

Appendix B

RESULTS OF ALL PHANTOMS

B.1 RESULT FROM PHANTOMS MADE WITH SILICIUM CARBIDE

Table B.1: *Summary of the results from phantoms made with silicium carbide (8.3-10.3 μm). Number of* $190\mu m$ *particles indicated but only approximate values were given to the number of* $100\mu m$ *calcium particles because it was hard to count them.*

Phantom	**μCa /[μm]**	**comments**
A	-	Full of clumps
B	-	Inadequate scatterers
C	-	Inadequate scatterers
D	?/190	Air bubbles at the layer
E	?/190	Air bubbles at the layer
F	?/190	Full of air bubbles
G	-	Air bubbles at the layer
H	-	Air bubbles at the layer
I	7/190	Full of air bubbles
J	-	Air bubbles at the layer
K	-	No air bubbles at layer (Good phantom)
L	-	Large air bubbles
M	8/190	No air bubbles at layer (Good phantom)
N	?/190	Lots of calcium particles
O	∼20/100	No air bubbles at layer (Good phantom)
P	8/190	Few air bubbles in phantom
Q	∼20/100	Few air bubbles in phantom

B.2 RESULTS FROM PHANTOMS MADE WITH SEPHADEX

Table B.2: *Summary of the results from phantoms made with sephadex (20-80 μm). Number of* $190\mu m$ *particles indicated but only approximate values were given to the number of* $100\mu m$ *calcium particles because it was hard to count them.*

Phantom	**μCa /[μm]**	**comments**
R	-	Homogeneous but not adequate background scattering on sonograph
S	-	Homogeneous but not adequate background scattering on sonograph
T	8/190	Homogeneous but not adequate background scattering on sonograph
U	6/190	Lot of air bubbles although sonograph shows homogeneous background scattering
V	8/190	Background scattering not as good as U
W	5/190	Homogeneous but not adequate background scattering (particle could still be seen as in M)
X	6/190	Homogeneous but not adequate background scattering (particle could still be seen as in M)
Y	∼50/100	Homogeneous but not adequate background scattering on sonograph
Z	8/190	Homogeneous but not adequate background scattering on sonograph
Æ	-	Homogeneous but not adequate background scattering on sonograph
A2	8/190	No bubbles at layer with adequate background scattering (good phantom)
B2	-	No bubbles at layer with adequate background scattering (good phantom)
C2	∼40/100	No bubbles at layer with adequate background scattering (good phantom)
D2	8/190	Homogeneous and adequate background scattering but layer separated into two

Bibliography

[1] G. M. Tse, P. H. Tan, A. L. Pang, A. P. Tang, and H. S. Cheung. "Calcification in breast lesions-pathologist' perspective". *Journal of Clinical Pathology*, 60:1–26, 2007.

[2] W. T. Yang, M. Suen, A. Ahuja, and C. Metreweli. "In vivo demonstration of microcalcification in breast cancer using high resolution ultrasound". *The British Journal of Radiology*, 70:685–690, 1997.

[3] R. F. Chang, S. F. Huang, L. P. Wang, D. R. Chen, and W. K. Moon. "Microcalcification detection in 3-d breast ultrasound". In *Engineering and Medicine and Biology 27th conference*, pages 6297–6300, September 2006.

[4] T. M. Kolb, J. Lichy, and J. H. Newhouse. "Occult cancer in women with dense breasts:detection with screening us-diagnostic yield and tumor characteristics". *Radiology*, 207:191–199, 1998.

[5] W. K. Moon, J. G Im, Y. H. Koh, D. Y Noh, and I. A. Park. "Ultrasound of mammographically metected clustered microcalcifications". *Radiology*, 217:849–854, 2000.

[6] T. Nagashima, H. Hashimoto, K. Oshida, S. Nakano, N. Tanabe, T. Nikaido, K. Koda, and M. Miyazaki. "Ultrasound demonstration of mammographically detected microcalcifications in patients with ductal carcinoma in situ of the the breast". *Breast Cancer*, 12:216–220, 2005.

[7] S. S. Kang. "Breast us in patients who had microcalcifications with low concern malignancy on screening mammograpy". *European Journal of Radiology*, 35:1–7, 2007.

[8] V. Londero, C. Zuiani, A. Furlan, J. Nori, and M. Bazzochi. "Role of ultrasound and sonographically guided core biopsy in the diagnostic evaluation of ductal carcinoma in situ(dcis) of the breast". *Radiologia medica*, 112:863–876, 2007.

[9] B. A. J. Angelsen and R. Hansen. "Surf imaging-a new method for ultrasound contrast agent imaging". *IEEE Ultrasonics Symp. New York*, pages 1–11, 2007.

[10] K. Armstrong, E. Moye, S. Williams, J. A. Berlin, and E. E. Reynolds. "Screening mammography in women 40 to 49 years of age: a systematic review for the american college of physicians". *Annals of Internal Medicine*, 146:516–526, 2007.

[11] MedicneNet.com. http://www.medicinenet.com/breast_cancer/page3.

[12] World Health Organization. http://www.who.int/mediacentre/factsheets/fs297 /en/index.html. Fact sheetNo. 297.

[13] Macafem: Women Health Network. http://www.womens-health-issues.info/breast-cancer-information.htm.

[14] P. Rosen. *Rosen's Breast Pathology.* Lippincott Williams & Wilkins,Philadelphia, New York Presbyterian Hospital-Cornell Medical Center. New York, 2nd edition edition, 2001.

[15] D. Kopans. *Breast Imaging.* Lippincott Williams& Wilkins, 2006.

[16] O. Peart. *Mammography and Breast Imaging:Just the Facts.* McGraw-Hill Medical Publishing Division, New York, 2005.

[17] D. T. Ramsay, J. C. Kent, R. A. Hartmann, and P. E. Hartmann. "Anatomy of the lactating human breast redefined with ultrasound imaging". *Journal of Anatomy*, 206:525–534, 1986.

[18] M. A. Henderson. "Clinical approach to the patient to the patient with a breast complaint". www.surgerystv.unimelb.edu.au/mah/branatindex.htm, 2006.

[19] D. Hayes. *Atlas of Breast Cancer.* Mosby, 2nd edition edition, 2000.

[20] S. F. McGee1, F. Lanigan1, E. Gilligan1, and B. Groner, editors. *Mammary Gland Biology and Breast Cancer*, volume 7. European Molecular Biology Organization (EMBO) Molecular Medicine, June 2006.

[21] L. J. Kleinsmith. *Principles of Cancer Biology.* Pearson Benjamin Cummings, San Francisco, 2006.

[22] M. Slatter, S. Danieletto, M. Pooley, L. C.Teh, A. G. Baird, and J. A. Barden. "Differentiation between cancerous and normal hyperplastic lobules in breast lesions". *Breast Cancer Research and Treatment*, 83:1–10, 2004.

[23] C. G. Begley and M. Braun. "General pathology: fibroadenoma of the breast". http://www.opt.indiana.edu/v543/slides/97af.html, November 1998.

[24] D. R. Lannin, A. K. Konstantakos, and J. H. Raaf. "Cystosarcoma phyllodes". http://www.emedicine.com/med/topic500.htm, June 2006.

[25] S. Z. Ali. "An atlas of breast images: histopathology and cytopathology". www.hopkinsbreastcenter.org/pathology/benign/, 2007.

[26] Breastcancer.org. http://www.breastcancer.org/pictures/types/index.

[27] P. H. Tan, B. B Goh, G. Chiang, and B. H. Bay. "Correlation of nuclear morphometry with pathologic in ductal carcinoma in situ of the breast". *Modern Pathology*, 14:937–941, 2001.

[28] H. Burstein, K. Polyak, J. S. Wong, S. C. Lester, and C. M. Kaelin. "Ductal carcinoma in situ of the breast". *New England Journal of Medicine*, 350:1430–1441, 2004.

[29] O. B. Ioffe and S. G. Silverberg. *Atlas of Breast Pathology*, chapter 10, pages 117–137. Pa: WB Saunders, Philadelphia, New York, 2nd edition edition, 2002.

[30] S. R .Lakhani. "The pathology of familial breast cancer: morphological aspects". *Breast Cancer Research*, 1:31–35, 1999.

[31] Cancerbackup-UK. http://www.cancerbackup.org.uk/Aboutcancer/Precancerousconditions/Breastcalcifications.

[32] T. W. Stephens and G. J. Whitman. "Breast:benign calcifications". http://www.emedicine.com/radio/topic880.htm, March 2005.

[33] W. K. Moon, J. S. Myung, Y. J. Lee, I. A. Park, D. Y. Noh, and J. G. Im. "Us of ductal carcinoma in situ". *RadioGraphics*, 22:269–281, 2002.

[34] B. A. J. Angelsen. *Waves, Signals, and Siginal Processing.* Trondheim Emantec, 2000.

[35] P. N. T.Wells. "Ultrasound imaging". *Physics in Medicine and Biology*, 51:83–98, 2006.

[36] S. P. Nasholm. *"Transmit beams adapted to multiple scattering noise suppression using a dual-frequency technique"*. PhD thesis, Norwegian University of Science and Technology (NTNU), Department of Circulation and Imaging. NTNU Trondheim, Norway(peter.nasholm@ntnu.no), 2007.

[37] S. E. Måsøy, Ø. Standal, P. Nasholm, T. F. Johansen, B. A. J. Angelsen, and R. Hansen. "Imaging: In vivo demonstration of an ultrasound contrast agent detection technique". Not yet published, 2007.

[38] R. Hansen, T. F. Johansen, and B. A. J. Angelsen. "Improving contrast agent detection by surf imaging. theoretical considerations and initial in vitro experiments". Not yet published.

[39] S. V. W. Hilton, G. R. Leopold1, L. K. Olson1, and S. A. WiIlson. 'Real-time breast sonograph: application in 300 consecutive patients". *American Journal of Roentgenology*, 147:479–486, 1986.

[40] M. S. Soo, J. A. Baker, and E. L. Rosen. "Sonographic detection and sonographically guided biopsy of breast microcalcifications". *American Journal of Roentgenology*, 180:941–948, 2003.

[41] S. E. Måsøy. Personal communication, 2007.

[42] United States Patent 5902748. Method of making a solid tissue mimicking material for ultrasound phantoms. http://www.freepatentsonline.com.5902748html, 1995. Application Ser. No.08/449.755.

[43] K. E. Fredfeldt. "An easily made ultrasound biopsy phantom". *Breast Cancer Research and Treatment*, 5:295–297, 1986.

[44] I. L. Hilde. "Framstilling av ultralydfantom: biopsy phantoms". Technical report, Norwegian University of Science and Technology (NTNU), Faculty of Medicine; Department of Circulation and Imaging, 2006.